National Library of Canada
Acquisitions and Bibliographic Services Branch
395 Wellington Street
Ottawa, Ontario
K1A 0N4

Bibliothèque nationale du Canada
Direction des acquisitions et des services bibliographiques
395, rue Wellington
Ottawa (Ontario)
K1A 0N4

Your file Votre référence

Our file Notre référence

NOTICE

The quality of this microform is heavily dependent upon the quality of the original thesis submitted for microfilming. Every effort has been made to ensure the highest quality of reproduction possible.

If pages are missing, contact the university which granted the degree.

Some pages may have indistinct print especially if the original pages were typed with a poor typewriter ribbon or if the university sent us an inferior photocopy.

AVIS

La qualité de cette microforme dépend grandement de la qualité de la thèse soumise au microfilmage. Nous avons tout fait pour assurer une qualité supérieure de reproduction.

S'il manque des pages, veuillez communiquer avec l'université qui a conféré le grade.

La qualité d'impression de certaines pages peut laisser à désirer, surtout si les pages originales ont été dactylographiées à l'aide d'un ruban usé ou si l'université nous a fait parvenir une photocopie de qualité inférieure.

Canada

ANALYTICAL ANALYSIS OF THE FREE VIBRATION OF PARTIALLY CLAMPED CANTILEVER PLATES

Thesis Submitted to the School of Graduate Studies as Partial Fulfillment of the Requirements for the Degree of Master of Applied Science

SARAH XOCHITL FULFORD

Department of Mechanical Engineering
University of Ottawa
Ottawa, Ontario, January 1994

ISBN 0-315-95922-3

Canada

UNIVERSITÉ D'OTTAWA
UNIVERSITY OF OTTAWA

ABSTRACT

The method of superposition is used to analyze the free vibration of thin rectangular plates, partially clamped along one edge and free everywhere else. This study has been undertaken because of interest in the dynamic behaviour of electronic circuit boards which are sometimes given support of this nature. This problem is not known to have been studied before using an analytical type method. Eight building blocks are superimposed to obtain the final solution. Each building block is solved individually using the Lévy-type solution. A detailed mathematical development of the solution is shown for each building block in dimensionless form. The natural frequencies and mode shapes for plates with varying aspect ratios and clamped lengths can be found using this method. Eigenvalues are shown to converge and tabulated values are given to at least three digit accuracy. Frequencies and mode shapes agree very well with experimentally found results and with results found using a commercially used finite element method software package.

ACKNOWLEDGEMENTS

I would like to offer my sincere thanks to various individuals who helped me make this work possible. My thesis supervisor, Professor D.J.Gorman, has been very accessible to me. Without his years of experience in the field of plate vibration and his willingness to instruct me, this work would not have been possible. I appreciate also the work done by R.K. Singhal from the Canadian Space Agency to provide me with experimental data. I must also thank my friend Levino Caravaggio from SPAR Aerospace who provided me with finite element data to further validate my results. I value the technical help contributed by my colleagues K.V. Nguyen and D. Michellussi. Finally, I sincerely thank my sister, Martha Fulford, and my close friend, Maha Masri, for their help and moral support.

TABLE OF CONTENTS

NOTATIONS

a	plate lateral dimension
b	plate lateral dimension
D	$= Eh^3/[12(1-\nu^2)]$, plate flexural rigidity
E	Young's modulus of the plate material
f	plate vibration frequency (hertz)
h	plate thickness
$q(x,y)$	lateral loading of the plate surface
t	time (seconds)
$W(\xi,,\eta,t)$	plate lateral displacement
$W(\xi,,\eta)$	amplitude of the plate lateral displacement
$x,,y$	plate spatial coordinates
λ^2	$= \omega a^2(\rho/D)^{1/2}$, plate eigenvalue
ρ	plate density
ω	circular frequency of plate vibration
ϕ	$= b/a$, plate aspect ratio
ν	Poison's ratio for the plate Material
ν^*	$= 2-\nu$
ξ	$= x/a$, dimensionless plate spatial coordinate
η	$= y/b$,dimensionless plate spatial coordinate
β	plate solution parameter (defined in text)
γ	plate solution parameter (defined in text)

Δ	increment size for eigenvalue iteration
ε_x	strain in the x-direction
ε_y	strain in the y-direction
r_x	radius of curvature in the x-z plane
r_y	radius of curvature in the y-z plane
κ	curvature
M	moment
V	vertical edge reaction
α	dimensionless clamped length
K	number of terms in the solution summation
KL	number of terms in the Dirac delta summation

Chapter 1: Introduction

1.1: Problem Definition

There exists several discrete frequencies for which an external force will cause an object to undergo large-amplitude vibrations. This phenomenon is called resonance. The discrete frequencies are known as resonant frequencies or natural frequencies of vibration. At each natural frequency the object will have a characteristic shape known as the mode shape. The aim of this research is to find an analytical-type solution for the free vibration of rectangular plates partially clamped along one edge. The plate is shown schematically in Figures 1.1. The plate is free on three edges and part of the fourth edge

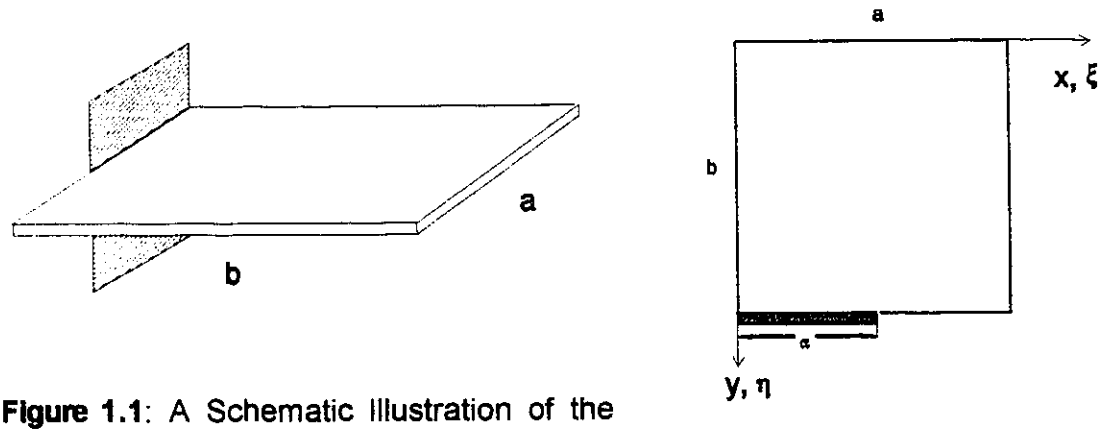

Figure 1.1: A Schematic Illustration of the Partially Clamped Cantilever Plate

and then clamped on the remaining portion of the fourth edge. Solutions for the resonant free vibration frequencies and mode shapes of thin rectangular plates with combinations of classical edge conditions are well established. Plate vibration problems with mixed boundary conditions (discontinuities in the edge support) are rarely dealt with using analytical techniques. The method to be used is the superposition method developed, as an extension of earlier work, by D.J. Gorman at the university of Ottawa [1]. This method has been shown to be powerful for solving free vibration problems and has the potential for use in other types of problems such as stress analyses. The method is referred to as being an analytical-type method of solution because it is closed form as an infinite series. If it were possible to sum infinity terms then the solutions would be exact. Although it is of course necessary to truncate the series it can be done at any desired degree of accuracy. If made a little more accessible, this method could be a useful corroborating tool for results obtained from numerical methods such as those found using the finite element method or the boundary element method.

The study of the partially clamped cantilever plate has been undertaken because of an interest in the dynamic behaviour of electronic circuit boards which are sometimes given support of this nature. Knowing the natural frequencies and mode shapes enables the designer to prolong the fatigue life of the board and the mounted components. The circuit board should be designed so that the natural frequency is out of range of any driving frequency. Mode shape data can be used to avoid placing delicate components on points of high displacement.

1.2: Literature Review

Many researchers using a variety of techniques have successfully analyzed the free vibration of thin rectangular plates with combinations of classical edge conditions [2] [1] [3] [4]. The situation, however, of discontinuous or mixed boundary conditions on the edges of a freely vibrating plate has not received very much attention. Results of the specific case of the partially clamped cantilever plate are not known to the author to have been published. Solutions to the general case of plates of arbitrary shape and boundary conditions have been approximated by finite element methods and boundary element methods [5-8].

There are generally two requirements in thin plate analysis, the governing differential equation and the prescribed boundary conditions must be satisfied. A variety of mathematical techniques have been employed to accomplish these tasks. The well known governing differential equation for static plate problems is credited to Lagrange (1811) [2]. This equation was modified slightly for application to free vibration problems. It will be developed fully in chapter 3. The background theory for this work was obtained almost exclusively from Timoshenko's classic text on the theory of plates and shells [2].

A few important researchers should be mentioned for having produced comprehensive studies of free vibration problems and thus are frequently used to compare data. Leissa's book [4] on the vibration of plates has compiled earlier work and developed solutions to a wide range of plate problems of varying shapes and boundary conditions. For rectangular plate analysis, Leissa generally uses the Rayleigh method of assuming the deflection function as a product of beam functions. Leissa does not deal

with mixed boundary condition problems. Nowacki [3] gives a solution to one example of a plate with discontinuous boundary conditions, a partially clamped simply supported plate with in-plane forces. The solution he provides is approximate. Nowacki cites other authors (Z. Kaczkowski and S. Kaliski) who have worked on discontinuous boundary value problems, however, there work is available only in Polish.

The Raleigh Ritz method makes use of the maximum strain energy and maximum kinetic energy of the plate. This method has been used in many problems [9-10], however, it has limitations for studies of plates with free edges. Bassily and Dickinson [11] discuss this problem.

The finite element method has been very successful in the area of plate vibration analysis. The FEM involves discretizing the numerical solution domain. There are numerous publications demonstrating the use of this method for plate vibration problems. References [7] and [9] are just two examples. Commercial software packages are also available which have the capability to solve resonant frequencies and mode shapes of thin plates with arbitrary shapes and boundary conditions. Although this method is powerful, it is an approximation and incorrect results may be obtained if the elements are poorly chosen. There is thus a definite need for analytical solutions to verify the results.

The boundary element method, BEM, is another numerical method which has attracted attention in recent years. The characteristic feature of the method is that only the boundary of the solution domain need be modelled. This leads to a relatively smaller set of resulting algebraic equations when compared to the FEM. It makes use of the basic equations of elastodynamics and dynamic reciprocal theorems [12]. The BEM has

been used for eigenvalue analysis of two dimensional and three dimensional problems described in reference [5] and [6]. The validity of the results obtained are checked by comparing to available analytical results.

The present work uses analytical methods of solution. A combination of Lévy-type [1] solutions and the superposition method developed by D.J. Gorman [2] is used. The method is an extension of the mathematical approach used in reference [13] which solves the partially clamped simply supported plate and the partially clamped partially free, simply supported plate. These plate problems are less complex then the ones solved here. The solution to the completely free plate, found earlier by Gorman [14], was also used for the partially clamped plate problem. The experimental procedure described in reference [14] was employed by R.K. Singhal from the Canadian Space Agency to verify the results obtained.

Chapter 2: Underlying Theory

2.1: Assumptions and Mathematical Formulation of the Bending Moments

A fundamental feature of the mathematical formulations involved in the thin plate theory used here, is that all of the necessary equations are derived in terms of only one variable, the lateral deflection, w. These formulations are subject to certain assumptions which should be made clear at the outset of this analysis. The assumptions will be stated here and referred to when significant to any portion of the mathematical formulation of the classical boundary conditions [1].

Assumptions:

1. The middle plane of the plate remains neutral during bending, that is, it does not undergo any extension.
2. Points of the plate lying initially on a normal-to-the-middle plane of the plate remain on the normal-to-the-middle surface of the plate after bending.
3. The normal stresses in the direction transverse to the plate, σ_z, can be disregarded.
4. The load acting on the plate is normal to its surface.
5. The deflections are small in comparison with the thickness of the plate.
6. The plate edges are free to move in the plane of the plate at the boundary.
7. The material used is isotropic.

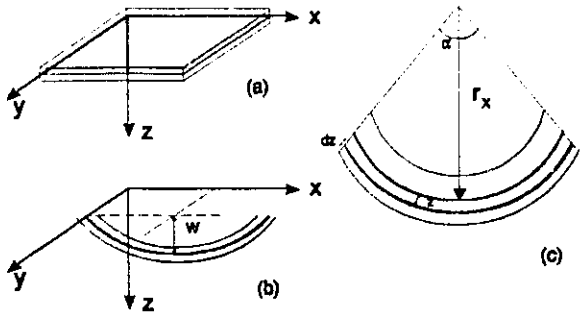

Figure 2.1: Coordinate System Definition

The coordinate system to be used is illustrated in Figure 2.1a. The middle plane of the plate before bending occurs is taken as the xy plane. The thickness of the plate, h, will start from z=-h/2 to z=h/2. The defection, w, is the displacement of the middle plane of the plate after bending (Fig 2.1b).

From assumption 1., it is possible to find the strains, ε_x and ε_y, after bending, of any plane of the plate a distance z from the neutral plane. The unit elongation of the plane shown in the element illustrated in Figure 2.1c, is given by,

$$\epsilon_x = \frac{\alpha(r_x + z) - \alpha r_x}{\alpha r_x} \tag{2.1}$$

where, r_x is the radius of curvature parallel to the x-axis and α is the angle sustained. After simplifying we get,

$$\epsilon_x = \frac{z}{r_x} \tag{2.2}$$

and similarly,

$$\epsilon_y = \frac{z}{r_y} \tag{2.3}$$

The reciprocal of the radius of curvature, known as the curvature, κ, is described mathematically as,

$$\kappa_x = \frac{1}{r_x} = \frac{\left|\frac{\partial^2 w}{\partial x^2}\right|}{[1+(\frac{\partial w}{\partial x})^2]^{3/2}} \tag{2.4}$$

Since we are dealing with only small deflection (assumption 5.), the higher order terms in the denominator can be neglected, leaving

$$\kappa_x = \frac{1}{r_x} = -\frac{\partial^2 w}{\partial x^2} \tag{2.5}$$

and similarly

$$\kappa_y = \frac{1}{r_y} = -\frac{\partial^2 w}{\partial y^2} \tag{2.6}$$

The negative sign is introduced because we consider a positive curvature to be convex downward and the second derivatives, $\partial^2 w/\partial x^2$ and $\partial^2 w/\partial y^2$ are negative [2 p.34].

Given the above relationships, it is now possible to express the normal stresses acting on the plate in terms of *w*, by making use of Hook's law and assumption 3,

$$\sigma_x = \frac{-Ez}{1-\nu^2}\left(\frac{\partial^2 w}{\partial x^2} + \nu\frac{\partial^2 w}{\partial y^2}\right) \tag{2.7}$$

$$\sigma_y = \frac{-Ez}{1-\nu^2}\left(\frac{\partial^2 w}{\partial y^2} + \nu\frac{\partial^2 w}{\partial x^2}\right) \tag{2.8}$$

Where the Young's modulus, E, and poisson's ratio, ν, are both material constants [2 p.39]. The external moments per unit length, M_x and M_y, can be obtain by integrating the stress times the distance from the mid-plane, over the thickness.

$$M_x = \int_{-h/2}^{h/2} \sigma_x \, z dz = -D\left(\frac{\partial^2 w}{\partial x^2} + \nu\frac{\partial^2 w}{\partial y^2}\right) \tag{2.9}$$

$$M_y = \int_{-h/2}^{h/2} \sigma_y \, z dz = -D\left(\frac{\partial^2 w}{\partial y^2} + \nu\frac{\partial^2 w}{\partial x^2}\right) \tag{2.10}$$

Where D is the flexural rigidity defined as

$$D = \frac{Eh^3}{12(1-\nu^2)} \tag{2.11}$$

Letting u and v denote the displacements in the x and y directions, the shearing strain is given by

$$\gamma_{xy} = \frac{\partial u}{\partial y} + \frac{\partial v}{\partial x} \tag{2.12}$$

The shearing stress is

$$\tau_{xy}=G(\frac{\partial u}{\partial y}+\frac{\partial v}{\partial x}) \qquad \textbf{(2.13)}$$

Figure 2.2 shows a counter-clockwise rotation of an element pq in the xz plane, which was originally perpendicular to the xy plane.

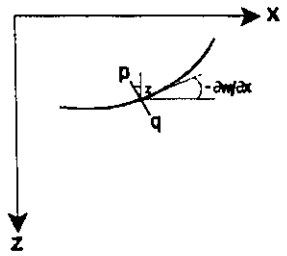

Figure 2.2: Rotation of an Element pq

The angle of rotation is -∂w/∂x so that the displacement u of a point on this element is

$$u=-z\frac{\partial w}{\partial x} \qquad \textbf{(2.14)}$$

similarly,

$$v=-z\frac{\partial w}{\partial y} \qquad \textbf{(2.15)}$$

substituting these values into equation 2.13 gives

$$\tau_{xy}=-2Gz\frac{\partial^2 w}{\partial x \partial y} \qquad \textbf{(2.16)}$$

The twisting moment M_{xy} is found by integrating the shear stress over the thickness.

$$M_{xy} = -\int_{-h/2}^{h/2} \tau_{xy} z dz = \frac{Gh^3}{6} \frac{\partial^2 w}{\partial x \partial y} = D(1-\nu) \frac{\partial^2 w}{\partial x \partial y} \qquad (2.17)$$

2.2: The Governing Differential Equation

The governing differential equation (GDE) to be developed here is widely accepted and can be found in numerous publications on plate theory. The validity of the GDE is subject to the above stated assumptions. Figures 2.3a and b are differential elements of the plate showing all the moments and shearing forces used in the thin plate analysis.

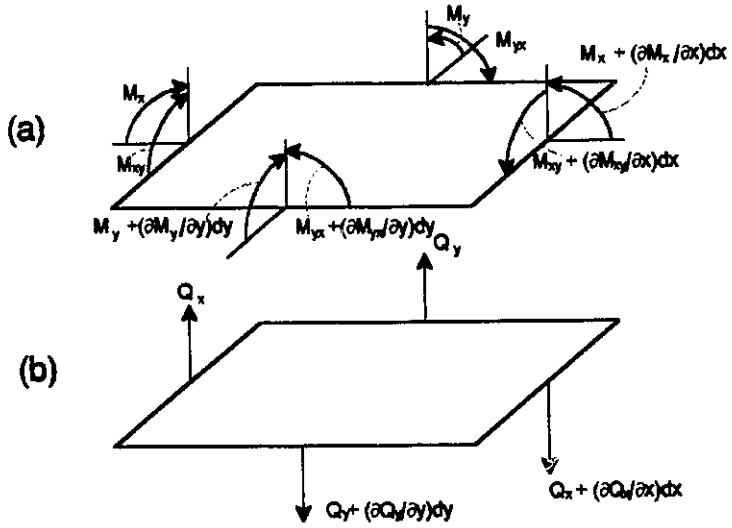

Figure 2.3: Differential Elements of The Plate

We also consider the intensity of the load, q, acting on the upper surface of the plate. From this, three equilibrium equations may be written by summing the forces in the z direction and summing the moments about the x and y axis, and setting them equal to

zero.

$$\frac{\partial Q_x}{\partial x}dxdy + \frac{\partial Q_y}{\partial y}dydx + qdxdy = 0 \qquad \textbf{(2.18)}$$

$$\frac{\partial M_{xy}}{\partial x}dxdy - \frac{\partial M_y}{\partial y}dydx + Q_y dxdy = 0 \qquad \textbf{(2.19)}$$

$$\frac{\partial M_{yx}}{\partial y}dxdy + \frac{\partial M_x}{\partial x}dxdy - Q_x dxdy = 0 \qquad \textbf{(2.20)}$$

The moments due to the load q, and the change in force Q_y and Q_x , are negligible. After dividing by the differential area dxdy, equations 18, 19 and 20 become,

$$\frac{\partial Q_x}{\partial x} + \frac{\partial Q_y}{\partial y} + q = 0 \qquad \textbf{(2.21)}$$

$$\frac{\partial M_{xy}}{\partial x} - \frac{\partial M_y}{\partial y} + Q_y = 0 \qquad \textbf{(2.22)}$$

$$\frac{\partial M_{yx}}{\partial y} + \frac{\partial M_x}{\partial x} - Q_x = 0 \qquad \textbf{(2.23)}$$

The three equations 2.21, 2.22, and 2.23 completely define the equilibrium of the element. These equations can be consolidated by solving for Q_y and Q_x in equations 2.22 and 2.23, then substituting into 2.21. This gives

$$\frac{\partial^2 M_x}{\partial x^2}+\frac{\partial^2 M_{yx}}{\partial x \partial y}+\frac{\partial^2 M_y}{\partial y^2}-\frac{\partial^2 M_{xy}}{\partial x \partial y}=-q \qquad \textbf{(2.24)}$$

Since $M_{yx}=-M_{xy}$ for equilibrium, we obtain

$$\frac{\partial^2 M_x}{\partial x^2}+\frac{\partial^2 M_y}{\partial y^2}-2\frac{\partial^2 M_{xy}}{\partial x \partial y}=-q \qquad \textbf{(2.25)}$$

Now, substituting the expression derived for M_x, M_y and M_{xy}, (equations 2.9, 2.10 and 2.17) we obtain,

$$\frac{\partial^4 w(x,y)}{\partial x^4}+2\frac{\partial^4 w(x,y)}{\partial x^2 \partial y^2}+\frac{\partial^4 w(x,y)}{\partial y^4}=\frac{q(x,y)}{D} \qquad \textbf{(2.26)}$$

In the case of freely vibrating plates, the surface loading term q(x,y) is replaced by an inertial force $\rho dA d^2w/dt^2$ which acts opposite to the displacement (now a function of position and time). Here, dA is an infinitesimal area and ρ is a mass per surface area. The governing differential equation becomes

$$\frac{\partial^4 w(x,y,t)}{\partial x^4}+2\frac{\partial^4 w(x,y,t)}{\partial x^2 \partial y^2}+\frac{\partial^4 w(x,y,t)}{\partial y^4}-\frac{\rho}{D}\frac{\partial^2 w(x,y,t)}{\partial t^2}=0 \qquad \textbf{(2.27)}$$

It is possible to express the displacement w(x,y,t) as a product of two functions, one a function of x and y and the other a function of time.

$$w(x,y,t)=W(x,y)\,T(t) \tag{2.28}$$

Substituting equation 2.28 into equation 2.27 and rearranging gives

$$\frac{D}{\rho}\left[\frac{\partial^4 W(x,y)}{\partial x^4}+2\frac{\partial^4 W(x,y)}{\partial x^2\partial y^2}+\frac{\partial^4 W(x,y)}{\partial y^4}\right]/W(x,y)=-\frac{d^2T(t)}{dt^2}/T(t) \tag{2.29}$$

Since the left hand side of equation 2.29 is a function of x and y only and the right hand side is a function of t only, both sides are equal to a constant. Setting the constant equal to the frequency squared, ω^2, gives

$$\frac{d^2T(t)}{dt^2}+\omega^2 T(t)=0 \tag{2.30}$$

$$\frac{\partial^4 W(x,y)}{\partial x^4}+2\frac{\partial^4 W(x,y)}{\partial x^2\partial y^2}+\frac{\partial^4 W(x,y)}{\partial y^4}-\frac{\omega^2\rho}{D}W(x,y)=0 \tag{2.31}$$

The solution to equation 2.30 is known to be

$$T(t)=A\,\sin(\omega t+\alpha) \tag{2.32}$$

Equation 2.31 is the governing differential equation to be solved by imposing prescribed

boundary conditions.

2.3: Boundary Conditions

2.3.1: Simply Supported

A simply supported plate edge is one which has zero displacement and zero moment about the edge direction. For an edge parallel to the y-axis , this is expressed from equation 2.9 as

$$w=0 \qquad \frac{\partial^2 w}{\partial x^2}+\nu\frac{\partial^2 w}{\partial y^2}=0 \Bigg|_{x=0,\ x=a} \tag{2.33}$$

Since $\partial^2 w/\partial y^2$ vanishes, this reduces to

$$w=0 \qquad \frac{\partial^2 w}{\partial x^2}=0 \Bigg|_{x=0,\ x=a} \tag{2.34}$$

For an edge parallel to the x-axis this becomes

$$w=0 \qquad \frac{\partial^2 w}{\partial y^2}=0 \Bigg|_{y=0,\ y=b} \tag{2.35}$$

2.3.2: Clamped

A clamped edge allows no displacement and no slope in the direction perpendicular to the edge. For an edge parallel to the y- axis,

$$w=0 \qquad \frac{\partial w}{\partial x}=0 \Big|_{x=0,\ x=a} \tag{2.36}$$

for an edge parallel to the x-axis

$$w=0 \qquad \frac{\partial w}{\partial y}=0 \Big|_{y=0,\ y=b} \tag{2.37}$$

2.3.3: Free

A free edge has no shearing force, no twisting moment and bending moment. The conditions of zero shearing force and zero twisting moment can be consolidated by observing that a distribution of twisting moment M_{xy} along an edge parallel to the y-axis is statically equivalent to a distribution of shearing forces of intensity [1 page 84]

$$Q_x'=-\left(\frac{\partial M_{xy}}{\partial y}\right) \Big|_{x=0,\ x=a} \tag{2.38}$$

The boundary condition is hence given by summing the shearing force and Q_x, and the Q_x' of equation 2.38 and setting them equal to zero, so that

$$V_x=\left(Q_x-\frac{\partial M_{xy}}{\partial y}\right)=0\Bigg|_{x=0,\ x=a} \tag{2.39}$$

or solving for Q_x in equation 2.23 and using M_{xy} given in equation 2.17 gives

$$\frac{\partial^3 w}{\partial x^3}+(2-\nu)\frac{\partial^3 w}{\partial x\partial y^2}=0\Bigg|_{x=0,\ x=a} \tag{2.40}$$

The condition of zero bending moment on an edge parallel to the y-axis is formulated from equation 2.9.

$$\frac{\partial^2 w}{\partial x^2}+\nu\frac{\partial^2 w}{\partial y^2}=0\Bigg|_{x=0,\ x=a} \tag{2.41}$$

Similarly, for edges parallel to the x-axis the conditions are

$$\frac{\partial^3 w}{\partial y^3}+(2-\nu)\frac{\partial^3 w}{\partial y\partial x^2}=0\Bigg|_{y=0,\ y=b} \tag{2.42}$$

$$\frac{\partial^2 w}{\partial y^2}+\nu\frac{\partial^2 w}{\partial x^2}=0\Bigg|_{y=0,\ y=b} \tag{2.43}$$

2.3.4: Slip Shear

The slip shear condition is one which is unlikely to be encountered on the edge of an actual plate but it is often used for analytical analysis [1 page 71]. The conditions are, zero vertical edge reaction and zero slope

$$\frac{\partial^3 w}{\partial x^3}+(2-\nu)\frac{\partial^3 w}{\partial x \partial y^2}=0 \Bigg|_{x=0,\ x=a} \tag{2.44}$$

$$\frac{\partial w}{\partial x}=0 \Bigg|_{x=0,\ x=a} \tag{2.45}$$

2.4: Non-Dimensionality

The governing differential equation 2.31, may be expressed in dimensionless form by introducing the dimensionless space variables, ξ and η, where ξ=x/a, η=y/b, a and b are the plate dimensions on the x and y edges respectively. Premultiplying and dividing the GDE by the quantities a and b gives [1 p.5]

$$\frac{a\partial^4 W(x,y)/a}{a^4\partial(x/a)^4}+\frac{2a\partial^4 W(x,y)/a}{a^2b^2\partial(x/a)^2\partial(y/b)^2}+\frac{a\partial^4 W(x,y)/a}{b^4\partial(y,b)^4}-\frac{a\omega^2\rho W(x,y)/a}{D}=0 \tag{2.46}$$

Now substituting ξ and η and the plate aspect ratio ϕ=a/b we obtain

$$\frac{\partial^4 W(\xi,\eta)}{\partial\xi^4}+\frac{2\partial^4 W(\xi,\eta)}{\phi^2\partial\xi^2\partial\eta^2}+\frac{\partial^4 W(\xi,\eta)}{\phi^4\partial\eta^4}-\lambda^4 W(\xi,\eta)=0 \tag{2.47}$$

where

$$\lambda^2=\omega a^2\sqrt{\rho/D} \tag{2.48}$$

A further simplification is given by multiplying equation 2.47 by ϕ^4, giving

$$\frac{\partial^4 W(\xi,\eta)}{\partial\eta^4}+2\phi^2\frac{\partial^4 W(\xi,\eta)}{\partial\eta^2\partial\xi^2}+\phi^4\frac{\partial^4 W(\xi,\eta)}{\partial\xi^4}-\phi^4\lambda^4 W(\xi,\eta)=0 \tag{2.49}$$

The same procedure can be used to express the classical boundary conditions in dimensionless form.

Simply Supported:

$$W(\xi,\eta) = \frac{\partial^2 W(\xi,\eta)}{\partial\xi^2} = 0\Big|_{\xi=0,\ \xi=1} \tag{2.50}$$

Clamped:

$$W(\xi,\eta) = \frac{\partial W(\xi,\eta)}{\partial\xi} = 0\Big|_{\xi=0,\ \xi=1} \tag{2.51}$$

Free:

$$\frac{\partial^2 W(\xi,\eta)}{\partial\xi^2} + \frac{\nu}{\phi^2}\frac{\partial^2 W(\xi,\eta)}{\partial\eta^2} = 0\Big|_{\xi=0,\ \xi=1} \tag{2.52}$$

$$\frac{\partial^3 W(\xi,\eta)}{\partial \xi^3} + \frac{\nu^*}{\phi^2} \frac{\partial^3 W(\xi,\eta)}{\partial \xi \partial \eta^2} = 0 \Big|_{\xi=0,\xi=1} \tag{2.53}$$

Slip Shear:

$$\frac{\partial W(\xi,\eta)}{\partial \xi} = 0 \Big|_{\xi=0,\ \xi=1} \tag{2.54}$$

$$\frac{\partial^3 W(\xi,\eta)}{\partial \xi^3} + \frac{\nu^*}{\phi^2} \frac{\partial^3 W(\xi,\eta)}{\partial \xi \partial \eta^2} = 0 \Big|_{\xi=0,\ \xi=1} \tag{2.55}$$

Other mathematical formulations important to the present work are that of distributed moments, vertical edge reactions and rotations along plate edges. In conventional coordinates a distributed bending moment acting perpendicular to the x and y axis is expressed as given in equation 2.9 and 2.10

$$M_x = -D\left(\frac{\partial^2 W}{\partial x^2} + \nu \frac{\partial^2 W}{\partial y^2}\right) \tag{2.56}$$

$$M_y = -D\left(\frac{\partial^2 W}{\partial y^2} + \nu \frac{\partial^2 W}{\partial x^2}\right) \tag{2.57}$$

In dimensionless form this becomes. [2 page 8]

$$\frac{M_\xi a}{D} = -\left[\frac{\partial^2 W(\xi,\eta)}{\partial \xi^2} + \frac{\nu}{\phi^2} \frac{\partial^2 W(\xi,\eta)}{\partial \eta^2} \right] \tag{2.58}$$

$$\frac{M_\eta \phi b}{D} = -\left[\frac{\partial^2 W(\xi,\eta)}{\partial \eta^2} + \nu \phi^2 \frac{\partial^2 W(\xi,\eta)}{\partial \xi^2} \right] \tag{2.59}$$

A distributed vertical edge reaction is given conventional coordinates is

$$V_x = -D \left(\frac{\partial^3 w}{\partial x^3} + \nu^* \frac{\partial^3 w}{\partial x \partial y^2} \right) \tag{2.60}$$

$$V_y = -D \left(\frac{\partial^3 w}{\partial y^3} + \nu^* \frac{\partial^3 w}{\partial y \partial x^2} \right) \tag{2.61}$$

and in dimensionless coordinates as [2 page 9]

$$\frac{V_\xi a}{D} = -\left[\frac{\partial^3 W(\xi,\eta)}{\partial \xi^3} + \frac{\nu^*}{\phi^2} \frac{\partial^3 W(\xi,\eta)}{\partial \xi \partial \eta^2} \right] \tag{2.62}$$

$$\frac{V_\eta \phi b}{D} = -\left[\frac{\partial^3 W(\xi,\eta)}{\partial \eta^3} + \nu^* \phi^2 \frac{\partial^3 W(\xi,\eta)}{\partial \eta \partial \xi^2}\right] \qquad \textbf{(2.63)}$$

2.5: Lévy-type Solutions for the Free Vibration of Rectangular Plates

When dealing with the bending of plates that have two opposite edges simply supported, M. Lévy suggested presenting a solution in the form,

$$W(\xi,\eta) = \sum_{m=1}^{\infty} Y_m(\eta) \sin m\pi\xi \qquad \textbf{(2.64)}$$

for plates with edges ξ=0 and ξ=1 simply supported. Y_m is a function of η only. It can be seen that this solution satisfies the simply supported boundary conditions. That is,

$$W(\xi,\eta) = \frac{\partial^2 W(\xi,\eta)}{\partial \xi^2} = 0 \quad \textit{at} \quad \xi = 0 \;,\; \xi = 1 \qquad \textbf{(2.65)}$$

The function $Y_m(\eta)$ must be found so as to solve the governing differential equation, and the boundary conditions at η=0 and η=1. This is done by substituting the solution into the governing differential equation 2.49, for vibration problems. This gives

$$\sum_{m=1}^{\infty}\left[\frac{d^4 Y_m(\eta)}{d\eta^4} - 2\phi^2 (m\pi)^2 \frac{d^2 Y_m(\eta)}{d\eta^2} + \phi^4\left[(m\pi)^4 - \lambda^4\right] Y_m(\eta)\right] \sin m\pi\xi = 0 \qquad \textbf{(2.66)}$$

Since each term of this series must identically equal zero, a fourth order homogeneous

differential equation is obtained as follows.

$$\frac{d^4Y_m(\eta)}{d\eta^4}-2\phi^2(m\pi)^2\frac{d^2Y_m(\eta)}{d\eta^2}+\phi^4[(m\pi)^4-\lambda^4]Y_m(\eta)=0 \qquad (2.67)$$

The solutions to this equation is, for $\lambda^2>(\pi m)^2$

$$Y_m(\eta)=A_m\cosh\ \beta_m\eta+B_m\sinh\ \beta_m\eta+C_m\sin\ \gamma_m\eta+D_m\cos\ \gamma_m\eta \qquad (2.68)$$

and for $\lambda^2<(m\pi)^2$,

$$Y_m(\eta)=A_m\cosh\ \beta_m\eta+B_m\sinh\ \beta_m\eta+C_m\sinh\ \gamma_m\eta+D_m\cosh\ \gamma_m\eta \qquad (2.69)$$

where

$$\beta_m=\phi\sqrt{\lambda^2+(m\pi)^2}\quad \gamma_m=\phi\sqrt{\lambda^2-(m\pi)^2}\quad ,\phi\sqrt{(m\pi)^2-\lambda^2} \qquad (2.70)$$

A_m, B_m, C_m and D_m are constants to be determined by enforcing the remaining four boundary conditions to be satisfied.

Lévy-type solutions can also be used for plate problems with two opposite edges having slip-shear conditions or opposite edges having slip-shear-simple-supported conditions. For two opposite edges having slip shear conditions, the solution is given as a cosine series.

$$W(\xi,\eta)=\sum_{m=0,1}^{\infty} Y_m(\eta)\cos m\pi\xi \qquad (2.71)$$

here,

$$\frac{\partial W(\xi,\eta)}{\partial \xi} = -\left[\frac{\partial^3 W(\xi,\eta)}{\partial \xi^3} + \nu^* \phi^2 \frac{\partial^3 W(\xi,\eta)}{\partial \xi \partial \eta^2}\right] = 0 \qquad (2.72)$$

For a plate having one edge simply supported and the opposite slip shear the solution may be given as

$$W(\xi,\eta) = \sum_{m=1,3,5}^{\infty} Y_m(\eta) \sin\frac{m\pi\xi}{2} \qquad (2.73)$$

The building blocks discussed in chapter 3 are all solved using Lévy-type solutions.

2.6: The Dirac Delta Function

The Dirac delta function is used extensively in chapter 3, in the formulation of solutions. To clarify those formulations, a definition is provided here as background. The Dirac delta function, often abbreviated as $\delta(x-x_0)$, has the following properties

$$1.\quad \delta(t-t_0) = \begin{cases} \infty, & t=t_0 \\ 0, & t\neq t_0 \end{cases}$$
$$2.\quad \int_{-\infty}^{\infty} \delta(t-t_0)\,dt = 1 \qquad (2.74)$$

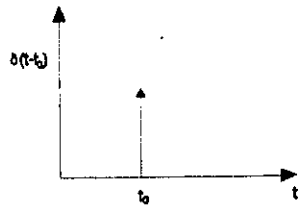

Figure 2.4: The Dirac Delta Function

An important result derived from these properties, is that for any function, f(x), continuous at $x=x_0$,

$$\int_{-\infty}^{\infty} \delta(x-x_0) f(x) dx = f(x_0) \tag{2.75}$$

The Dirac delta function is used in the work here to represent concentrated forces and moments. Expanded as a Fourier cosine series, the Dirac delta function takes the form

$$\delta(x-x_0) = a_0 + \sum_{m=1}^{\infty} a_m \cos\frac{2m\pi x}{T} \tag{2.76}$$

where T is the period,

$$a_0 = \frac{2}{T}\int_0^{T/2} \delta(x-x_0) dx \tag{2.77}$$

and

$$a_m=\frac{4}{T}\int_0^{T/2}\delta(x-x_o)\cos\frac{2m\pi x}{T}dx \qquad m=1,2,... \tag{2.78}$$

This gives, after integration

$$\delta(x-x_0)=1+\frac{4}{T}\sum_{m=1}^{\infty}\cos\frac{2m\pi x_0}{T}\cos\frac{2m\pi X}{T}dx \qquad m=1,2,.... \tag{2.79}$$

Using the previously defined space variables, ξ and η and introducing $\zeta=x_0/a$, the Dirac delta function can be written in dimensionless cosine series form [2]

$$\delta(\xi-\zeta)=2\sum_{m=0}^{\infty}\frac{\cos m\pi\zeta}{\alpha_m}\cos m\pi\xi \tag{2.80}$$

$$\alpha_m=\begin{cases}2, & m=0\\ 1, & m\neq 0\end{cases}$$

Chapter 3: The Superposition Method

3.1: Overview

The method used to analyze the free vibration of the partially clamped cantilever plate is the superposition method. This method involves solving separate plate problems ("building blocks") which when superimposed satisfy the desired boundary conditions.

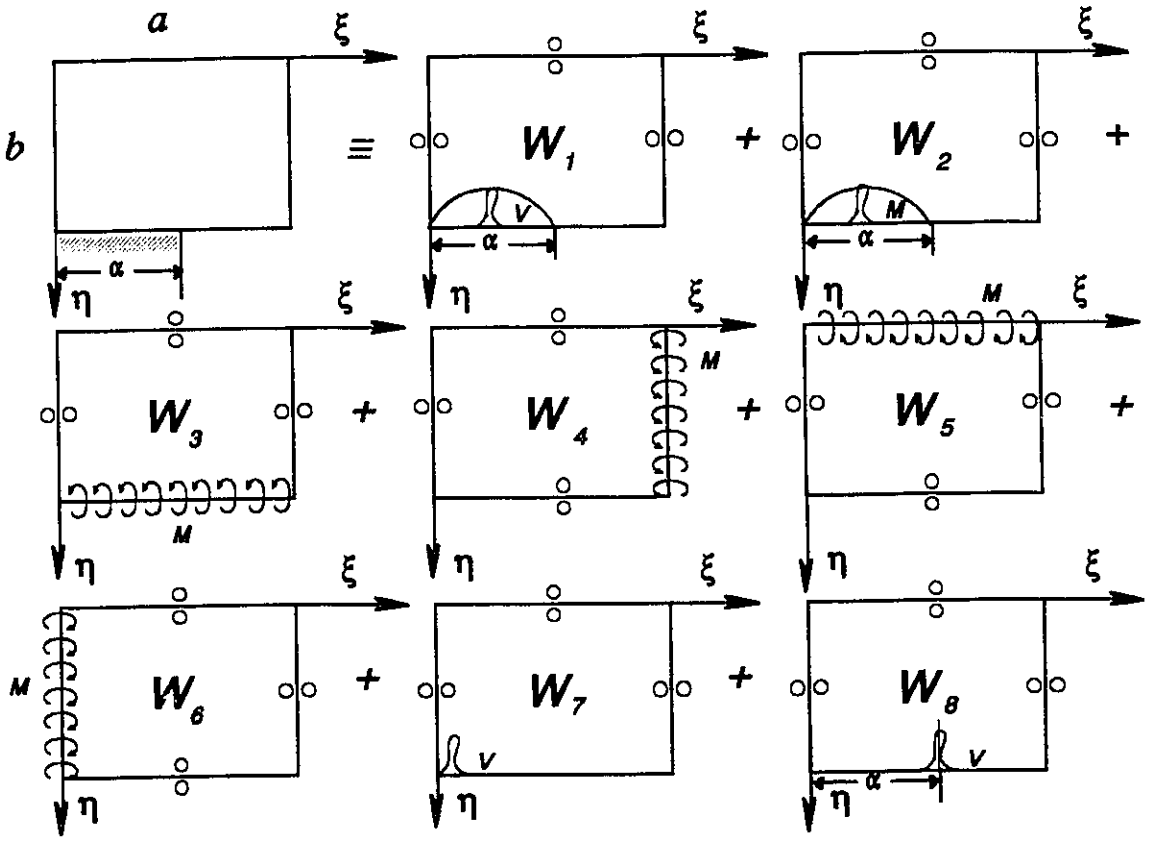

Figure 3.1: The Building Blocks

Individually each building block must satisfy the governing differentials equation, so their superposition will also satisfy the governing differential equation. The building blocks must be chosen so that when combined the final boundary conditions are attainable. The choice of building blocks is not unique as will be discussed further in chapter 6. Figure 3.1 shows the eight building blocks used here for the partially clamped cantilever plate. Each building block is individually solved using a Lévy-type method.

3.2: The Building Blocks

An explanation for the choice of building blocks will be given here, then in the subsequent sections of this chapter each building block will be individually solved. Referring again to Figure 3.1, it can be seen that the upper edge of the plate (η=0), for the partially clamped cantilever plate is free, that is, there is now bending moment or edge reaction. Now, considering the same edge on each of the building blocks, it can be seen that all but the fifth building block have slip shear conditions (zero edge reaction and zero slope) at the edge η=0. The fifth building block has an imposed distributed rotation and zero edge reaction. It can easily be seen that superimposing the given building blocks will automatically satisfy the condition of zero edge reactions by virtue of the fact that this condition is already independently satisfied by each of the building blocks. Considering the conditions of zero bending moment, it can be seen that each building block contributes bending moment so the distributed bending moment must be adjusted so that there is no net contribution. Similar logic can be used for the edges ξ=0 and ξ=1. The partially clamped edge, η=1, must have zero slope and displacement in

the region $0 \le \xi \le \alpha$ and free conditions in the region $\alpha \le \xi \le 1$. The building blocks 3 to 6 are adjusted so that together they contribute no moment or edge reaction. The first and second building blocks contribute no moment or edge reactions in the region $0 \le \xi \le \alpha$. The clamped portion can be adjusted so that the slope and displacement both cancel. The seventh and eighth building blocks provide a concentrated force at the extremities of the clamped region to counteract the effect of the twisting moment. Although there are eight building blocks, it will be shown that only the first three need be developed and the remainder can be extracted by substitutions.

3.2.1: Building Blocks 1 and 2

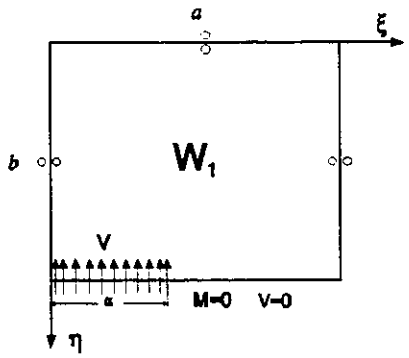

Figure 3.2: Building Block 1

Building block 1, shown in Figure 3.2, has slip shear conditions on the edges $\eta=0$, $\xi=0$, $\xi=1$. The edge $\eta=1$ has a distributed edge reaction and zero moment in the region $0 \le \xi \le \alpha$ and free conditions in the region $\alpha \le \xi \le 1$. To solve these conditions we start by assuming the Lévy-type solution given in equation 2.72.

$$W(\xi,\eta)=\sum_{m=0,1}^{\infty} Y_m(\eta)\cos m\pi\xi \tag{3.1}$$

Substituting this into the governing differential equation 2.49 gives the fourth order homogeneous differential equation 2.67 with the known solutions as stated in chapter 2.

For $\lambda^2>(\pi m)^2$

$$Y_m(\eta)=A_m\cosh\beta_m\eta+B_m\sinh\beta_m\eta+C_m\sin\gamma_m\eta+D_m\cos\gamma_m\eta \tag{3.2}$$

and for $\lambda^2<(m\pi)^2$,

$$Y_m(\eta)=A_m\cosh\beta_m\eta+B_m\sinh\beta_m\eta+C_m\sinh\gamma_m\eta+D_m\cosh\gamma_m\eta \tag{3.3}$$

where

$$\beta_m=\phi\sqrt{\lambda^2+(m\pi)^2}\quad \gamma_m=\phi\sqrt{\lambda^2-(m\pi)^2}\quad ,\phi\sqrt{(m\pi)^2-\lambda^2} \tag{3.4}$$

A_m, B_m, C_m and D_m are constants to be determined by enforcing the remaining four boundary conditions to be satisfied.

Enforcing the two boundary conditions on the edge $\eta=0$,

$$\frac{\partial W(\xi,\eta)}{\partial\eta}=0\Big|_{\eta=0} \tag{3.5}$$

$$\frac{\partial^3 W(\xi,\eta)}{\partial \eta^3} + \nu^* \phi^2 \frac{\partial^3 W(\xi,\eta)}{\partial \eta \partial \xi^2} = 0 \Big|_{\eta=0} \tag{3.6}$$

The two sine term constants are eliminated leaving,

for $\lambda^2 > (\pi m)^2$

$$Y_m(\eta) = A_m \cosh \beta_m \eta + B_m \cos \gamma_m \eta \tag{3.7}$$

and for $\lambda^2 < (m\pi)^2$,

$$Y_m(\eta) = A_m \cosh \beta_m \eta + B_m \cosh \gamma_m \eta \tag{3.8}$$

Another constant can be solved for by enforcing the condition of $M(\eta)\phi b/D = 0$ at $\eta=1$

or

$$\frac{\partial^2 W(\xi,\eta)}{\partial \eta^2} + \nu \phi^2 \frac{\partial^2 W(\xi,\eta)}{\partial \xi^2} = 0 \Big|_{\eta=1} \tag{3.9}$$

After substitution and rearranging we obtain,

for $\lambda^2 > (\pi m)^2$

$$Y_m(\eta) = A_m [\cosh \beta_m \eta + \theta_{1m} \cos \gamma_m \eta] \tag{3.10}$$

and for $\lambda^2 < (m\pi)^2$,

$$Y_m(\eta) = A_m [\cosh \beta_m \eta + \theta_{2m} \cosh \gamma_m \eta] \tag{3.11}$$

where,

$$\theta_{1m} = \frac{(\beta_m^2 - \nu\phi^2(m\pi)^2)\ \cosh\beta_m}{(\gamma_m^2 + \nu\phi^2(m\pi)^2)\cos\gamma_m} \tag{3.12}$$

$$\theta_{2m} = \frac{(\beta_m^2 - \nu\phi^2(m\pi)^2)\ \cosh\beta_m}{-(\gamma_m^2 + \nu\phi^2(m\pi)^2)\cosh\gamma_m} \tag{3.13}$$

Now, we represent the driving force as a Dirac delta function,

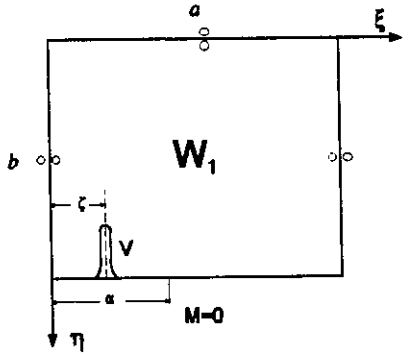

Figure 3.3: Driving Force as a Dirac Delta Function

$$\frac{V(\xi)b^2}{aD} = \sum_{m=0,1}^{\infty} \frac{2}{\delta_m}\cos\ m\pi\zeta\ \cos\ m\pi\xi \tag{3.14}$$

$$\delta_m = \begin{cases} 2, & m=0 \\ 1, & m\neq 0 \end{cases} \tag{3.15}$$

Since,

$$\frac{V(\xi)\phi b^2}{D} = -\left[\frac{\partial^3 W(\xi,\eta)}{\partial\eta^3} + \nu^*\phi^2 \frac{\partial^3 W(\xi,\eta)}{\partial\eta\,\partial\xi^2}\right] \tag{3.16}$$

we get at $\eta=1$ for $\lambda^2>(\pi m)^2$,

$$A_m = \frac{-2}{\delta_m}\frac{\cos\, m\pi\zeta}{\theta_{11m}} \tag{3.17}$$

and for $\lambda^2<(\pi m)^2$

$$A_m = \frac{-2}{\delta_m}\frac{\cos\, m\pi\zeta}{\theta_{22m}} \tag{3.18}$$

where

$$\theta_{11m} = \sinh\,\beta_m\,(\beta_m^3 - (m\pi)^2\nu^*\phi\beta_m) + \sin\,\gamma\,(\theta_{1m}\gamma_m^3 + (m\pi)^2\nu^*\theta_{1m}\gamma_m) \tag{3.19}$$

$$\theta_{22m} = \sinh\,\beta_m\,(\beta_m^3 - (m\pi)^2\nu^*\phi\beta_m) + \sinh\,\gamma\,(\theta_{2m}\gamma_m^3 - (m\pi)^2\nu^*\theta_{2m}\gamma_m) \tag{3.20}$$

Consider now, an infinity of Dirac delta functions with amplitudes distributed along the edge $\eta=0$, in the clamped region $0\le\xi\le\alpha$ (this is a mathematical procedure used often in electronics [21]).

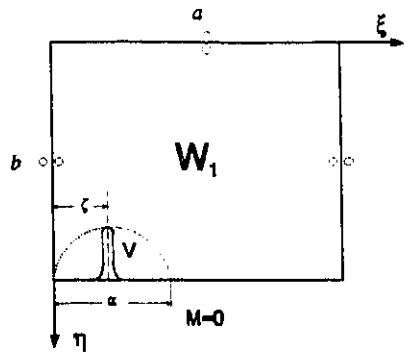

Figure 3.4: Envelope Infinity Dirac Delta Functions

Let the enveloping function be represented as a cosine series,

$$\frac{V(\zeta)b^2}{aD} = \sum_{j=0,1}^{\infty} E_j \cos\frac{j\pi\zeta}{\alpha} = amplitude(\zeta) \qquad (3.21)$$

Integrating from 0 to α and using the property shown in equation 2.75 we obtain,

$$A_m = \frac{-2}{\delta_m} \sum_{j=0,1}^{\infty} \frac{E_j}{\theta_{11m}} \int_0^{\alpha} \cos\frac{j\pi\zeta}{\alpha} \cos m\pi\zeta \, d\zeta \qquad (3.22)$$

$$A_m = \frac{-2}{\delta_m} \sum_{j=0,1}^{\infty} \frac{E_j}{\theta_{22m}} \int_0^{\alpha} \cos\frac{j\pi\zeta}{\alpha} \cos m\pi\zeta \, d\zeta \qquad (3.23)$$

If we denote,

$$\phi_{jm} = \int_0^{\infty} \cos\frac{j\pi\zeta}{\alpha} \cos m\pi\zeta \, d\zeta \qquad (3.24)$$

then we may reduce the expression for A_m to

$$A_m = \frac{-2}{\delta_m} \sum_{j=0,1}^{\infty} \frac{E_j}{\theta_{11m}} \phi_{jm} \tag{3.25}$$

$$A_m = \frac{-2}{\delta_m} \sum_{j=0,1}^{\infty} \frac{E_j}{\theta_{22m}} \phi_{jm} \tag{3.26}$$

The final solution for building block 1 is

$$\begin{aligned} W_1(\xi,\eta) = &\sum_{m=0,1}^{K^*} \frac{-2}{\delta_m} \sum_{j=0,1}^{\infty} \frac{E_j}{\theta_{11m}} \phi_{jm}(\cosh \beta_m\eta + \theta_{1m}\cos \gamma_m\eta)\cos m\pi\xi \\ &+ \sum_{K^*+1}^{\infty} \frac{-2}{\delta_m} \sum_{j=0,1}^{\infty} \frac{E_j}{\theta_{22m}} \phi_{jm}(\cosh \beta_m\eta + \theta_{2m}\cosh \gamma_m\eta)\cos m\pi\xi \end{aligned} \tag{3.27}$$

(Constants subscriped with 2 apply to the case where $\lambda^2<(m\pi)^2$)

Building block 2, shown in Figure 3.5, is very similar to building block 1. The only

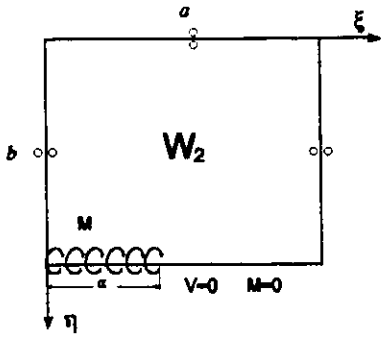

Figure 3.5: Building Block 2

difference is that instead of a distributed edge reaction, there is now a distributed moment in the region $0\leq\xi\leq\alpha$. Proceeding in the same manner as for the first building block from equation 3.1 to equation 3.8, we obtain as before for $\lambda^2>(\pi m)^2$

$$Y_m(\eta)=A_m\cosh\ \beta_m\eta+B_m\cos\ \gamma_m\eta \tag{3.28}$$

and for $\lambda^2<(m\pi)^2$,

$$Y_m(\eta)=A_m\cosh\ \beta_m\eta+B_m\cosh\ \gamma_m\eta \tag{3.29}$$

There are two constants to be determined and two boundary condition to be imposed along the edge $\eta=1$. There is zero edge reaction,

$$\frac{V_\eta\phi b}{D}=-\left[\frac{\partial^3 W(\xi,\eta)}{\partial\eta^3}+\nu^*\phi^2\ \frac{\partial^3 W(\xi,\eta)}{\partial\eta\,\partial\xi^2}\right]=0 \tag{3.30}$$

Substituting the solution thus far for $W(\xi,\eta)$ in equation 3.30 and setting $\eta=1$, makes it possible to solve for one of the constants. We obtain as before, for $\lambda^2>(\pi m)^2$

$$Y_m(\eta)=A_m[\cosh\ \beta_m\eta+\theta_{1m}\cos\ \gamma_m\eta] \tag{3.31}$$

and for $\lambda^2<(m\pi)^2$,

$$Y_m(\eta)=A_m[\cosh\ \beta_m\eta+\theta_{2m}\cosh\ \gamma_m\eta] \tag{3.32}$$

where,

$$\theta_{1m}=\frac{-(\beta_m^3-\beta_m\nu^*\phi^2(m\pi)^2)\ \sinh\beta_m}{(\gamma_m^3+\gamma_m\nu^*\phi^2(m\pi)^2)\sin\gamma_m} \tag{3.33}$$

$$\theta_{2m} = \frac{(\beta_m^3 - \beta_m \nu^* \phi^2 (m\pi)^2) \sinh \beta_m}{(\gamma_m^3 - \gamma_m \nu^* \phi^2 (m\pi)^2) \sinh \gamma_m} \tag{3.34}$$

Represent the moment as a Dirac delta function,

$$\frac{M(\xi)\phi b}{D} = \sum_{m=0,1}^{\infty} \frac{2}{\delta_m} \cos m\pi\zeta \cos m\pi\xi \tag{3.35}$$

$$\delta_m = \begin{cases} 2, & m=0 \\ 1, & m\neq 0 \end{cases} \tag{3.36}$$

Since,

$$\frac{M(\xi)\phi b}{D} = -\left[\frac{\partial^2 W(\xi,\eta)}{\partial \eta^2} + \nu\phi^2 \frac{\partial^2 W(\xi,\eta)}{\partial \xi^2} \right] \tag{3.37}$$

we get at $\eta=1$ for $\lambda^2>(\pi m)^2$,

$$A_m = \frac{-2}{\delta_m} \frac{\cos m\pi\zeta}{\theta_{11m}} \tag{3.38}$$

and for $\lambda^2<(\pi m)^2$

$$A_m = \frac{-2}{\delta_m} \frac{\cos m\pi\zeta}{\theta_{22m}} \tag{3.39}$$

where

$$\theta_{11m} = \cosh \beta_m (\beta_m^2 - (m\pi)^2 \nu\phi^2) - \cos \gamma_m (\theta_{1m}\gamma_m^2 + \theta_{1m}(m\pi)^2 \nu\phi^2) \tag{3.40}$$

$$\theta_{22m} = \cosh \beta_m (\beta_m^2 - (m\pi)^2 \nu\phi^2) + \cosh \gamma_m (\theta_{1m}\gamma_m^2 - \theta_{1m}(m\pi)^2 \nu\phi^2) \tag{3.41}$$

Consider now, an infinity of Dirac delta functions with amplitudes distributed along the edge η =0 in the region $0 \leq \xi \leq \alpha$.

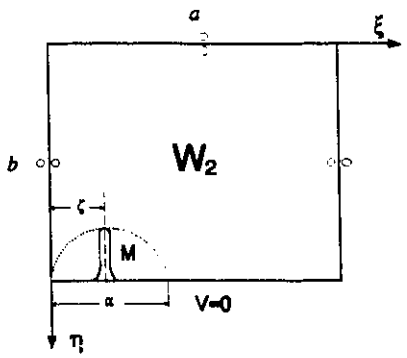

Figure 3.6: Envelope Infinity Dirac Delta Functions

Let the enveloping function be represented as a cosine series,

$$\frac{M(\zeta)\phi b}{D} = \sum_{j=0,1}^{\infty} E_j \cos\frac{j\pi\zeta}{\alpha} = amplitude(\zeta) \qquad (3.42)$$

Integrating from 0 to α and using the property shown in equation 2.75 we obtain,

$$A_m = \frac{-2}{\delta_m} \sum_{j=0,1}^{\infty} \frac{E_j}{\theta_{11m}} \int_0^{\alpha} \cos\frac{j\pi\zeta}{\alpha} \cos m\pi\zeta \, d\zeta \qquad (3.43)$$

$$A_m = \frac{-2}{\delta_m} \sum_{j=0,1}^{\infty} \frac{E_j}{\theta_{22m}} \int_0^{\alpha} \cos\frac{j\pi\zeta}{\alpha} \cos m\pi\zeta \, d\zeta \qquad (3.44)$$

If we denote,

$$\phi_{jm} = \int_0^{\infty} \cos\frac{j\pi\zeta}{\alpha} \cos m\pi\zeta \, d\zeta \qquad (3.45)$$

then we may reduce the expression for A_m to

$$A_m = \frac{-2}{\delta_m} \sum_{j=0,1}^{\infty} \frac{E_j}{\theta_{11m}} \phi_{jm} \tag{3.46}$$

$$A_m = \frac{-2}{\delta_m} \sum_{j=0,1}^{\infty} \frac{E_j}{\theta_{22m}} \phi_{jm} \tag{3.47}$$

The final solution for building block 2 is the same as that for building block 1 but the constants are defined differently.

$$\begin{aligned} W_2(\xi,\eta) = &\sum_{m=0,1}^{K^*} \frac{-2}{\delta_m} \sum_{j=0,1}^{\infty} \frac{E_j}{\theta_{11m}} \phi_{jm}(\cosh \beta_m\eta + \theta_{1m}\cos \gamma_m\eta)\cos m\pi\xi \\ &+ \sum_{K^*+1}^{\infty} \frac{-2}{\delta_m} \sum_{j=0,1}^{\infty} \frac{E_j}{\theta_{22m}} \phi_{jm}(\cosh \beta_m\eta + \theta_{2m}\cosh \gamma_m\eta)\cos m\pi\xi \end{aligned} \tag{3.48}$$

3.2.2: Building Blocks 3 to 6

The building blocks 3, 4, 5, and 6 differ only by their orientation (Figure 3.7). All four building blocks have slip shear conditions on three edges and a distributed harmonic rotation and zero edge reaction on the fourth edge. After solving one of the building blocks it will be shown that the remaining three can be extracted by simple substitutions. These building block have been solved before [13] for other plate problems. For the

present problem they are used exactly as for the completely fee plate problem. That is, the superposition of these building blocks contribute no bending moment or vertical edge reaction at the boundary. This will be demonstrated further when developing the eigenvalue matrix.

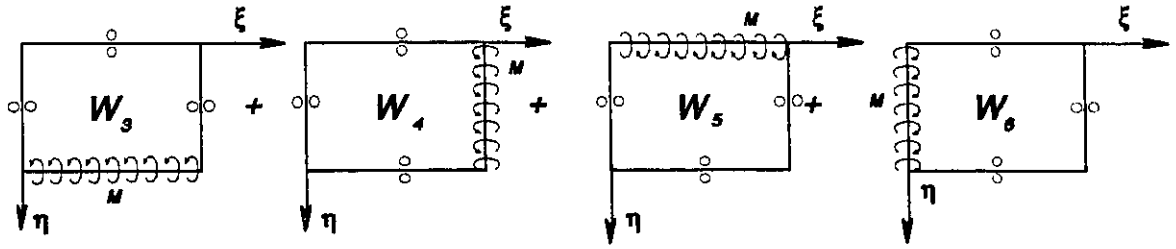

Figure 3.7: The Building Blocks 3, 4, 5 and 6

The solution to the first building block again begins with a Lévy-type formulation.

$$W(\xi,\eta)=\sum_{m=0,1}^{\infty} Y_m(\eta)\cos m\pi\xi \qquad (3.49)$$

The solution is continued exactly as it is done for the second building block from equation 3.28 to 3.34.

Now, letting the distributed harmonic rotation be represented as cosine series we get at η=1,

$$\frac{\partial W(\xi,\eta)}{\partial\eta}=\sum_{m=0,1}^{\infty} E_m\cos m\pi\xi \qquad (3.50)$$

or

$$\sum_{m=0,1}^{\infty} A_m \{\beta_m \sinh\beta_m - \theta_{1m}\gamma_m \sin\gamma_m\} \cos m\pi\xi = \sum_{m=0,1}^{\infty} E_m \cos m\pi\xi \qquad (3.51)$$

$$\sum_{m=0,1}^{\infty} A_m \{\beta_m \sinh\beta_m + \theta_{2m}\gamma_m \sinh\gamma_m\} \cos m\pi\xi = \sum_{m=0,1}^{\infty} E_m \cos m\pi\xi \qquad (3.52)$$

Thus,

$$A_m = \frac{E_m}{\beta_m \sinh\beta_m - \theta_{1m}\gamma_m \sin\gamma_m} \qquad (3.53)$$

$$A_m = \frac{E_m}{\beta_m \sinh\beta_m + \theta_{2m}\gamma_m \sinh\gamma_m} \qquad (3.54)$$

Introducing the constants

$$\theta_{11m} = \frac{1}{\beta_m - \dfrac{\theta_{1m}\gamma_m \sin\gamma_m}{\sinh\beta_m}} \qquad (3.55)$$

$$\theta_{13m} = \frac{\theta_{1m}\sin\gamma_m}{\sinh\beta_m \left[\beta_m - \dfrac{\theta_{1m}\gamma_m \sin\gamma_m}{\sinh\beta_m}\right]} \qquad (3.56)$$

and

$$\theta_{22m} = \frac{1}{\beta_m + \dfrac{\theta_{2m}\gamma_m \sinh\gamma_m}{\sinh\beta_m}} \qquad (3.57)$$

$$\theta_{23m}=\frac{\theta_{2m}\sinh\gamma_m}{\sinh\beta_m\left[\beta_m+\dfrac{\theta_{2m}\gamma_m\sinh\gamma_m}{\sinh\beta_m}\right]} \tag{3.58}$$

we obtain

$$Y_m(\eta)=E_m\left\{\theta_{11m}\frac{\cosh\beta_m\eta}{\sinh\beta_m}+\theta_{13m}\frac{\cos\gamma_m\eta}{\sin\gamma_m}\right\} \tag{3.59}$$

$$Y_m(\eta)=E_m\left\{\theta_{22m}\frac{\cosh\beta_m\eta}{\sinh\beta_m}+\theta_{23m}\frac{\cosh\gamma_m\eta}{\sinh\gamma_m}\right\} \tag{3.60}$$

The final solution is thus

$$\begin{aligned}W_3(\xi,\eta)=&\sum_{m=0,1}^{K^*}E_m\left\{\theta_{11m}\frac{\cosh\beta_m\eta}{\sinh\beta_m}+\theta_{13m}\frac{\cos\gamma_m\eta}{\sin\gamma_m}\right\}\cos m\pi\xi\\&+\sum_{K^*+1}^{\infty}E_m\left\{\theta_{22m}\frac{\cosh\beta_m\eta}{\sinh\beta_m}+\theta_{23m}\frac{\cosh\gamma_m\eta}{\sinh\gamma_m}\right\}\cos m\pi\xi\end{aligned} \tag{3.61}$$

To obtain the solution to building block 4 from the solution to the building block 3, the variables ξ and η are interchanged, ϕ is replaced by $1/\phi$ and λ^2 is replaced by $\lambda^2\phi^2$ [2] giving,

$$\begin{aligned}W_4(\xi,\eta)=&\sum_{m=0,1}^{K^*}E_m\left\{\theta_{11m}\frac{\cosh\beta_m\xi}{\sinh\beta_m}+\theta_{13m}\frac{\cos\gamma_m\xi}{\sin\gamma_m}\right\}\cos m\pi\eta\\&+\sum_{K^*+1}^{\infty}E_m\left\{\theta_{22m}\frac{\cosh\beta_m\xi}{\sinh\beta_m}+\theta_{23m}\frac{\cosh\gamma_m\xi}{\sinh\gamma_m}\right\}\cos m\pi\eta\end{aligned} \tag{3.62}$$

where,

$$\theta_{1m} = \frac{-(\beta_m^3 - \beta_m \nu^*(1/\phi^2)(m\pi)^2)\ \sinh\beta_m}{(\gamma_m^3 + \gamma_m \nu^*(1/\phi^2)(m\pi)^2)\sin\gamma_m} \tag{3.63}$$

$$\theta_{2m} = \frac{(\beta_m^3 - \beta_m \nu^*(1/\phi^2)(m\pi)^2)\ \sinh\beta_m}{(\gamma_m^3 - \gamma_m \nu^*(1/\phi^2)(m\pi)^2)\sinh\gamma_m} \tag{3.64}$$

$$\theta_{11m} = \frac{1}{\beta_m - \dfrac{\theta_{1m}\gamma_m \sin\gamma_m}{\sinh\beta_m}} \tag{3.65}$$

$$\theta_{13m} = \frac{\theta_{1m}\sin\gamma_m}{\sinh\beta_m \left[\beta_m - \dfrac{\theta_{1m}\gamma_m \sin\gamma_m}{\sinh\beta_m}\right]} \tag{3.66}$$

$$\theta_{22m} = \frac{1}{\beta_m + \dfrac{\theta_{2m}\gamma_m \sinh\gamma_m}{\sinh\beta_m}} \tag{3.67}$$

$$\theta_{23m} = \frac{\theta_{2m}\sinh\gamma_m}{\sinh\beta_m \left[\beta_m + \dfrac{\theta_{2m}\gamma_m \sinh\gamma_m}{\sinh\beta_m}\right]} \tag{3.68}$$

$$\beta_m=(1/\phi)\sqrt{\lambda^2\phi^2+(m\pi)^2}$$
$$\gamma_m=(1/\phi)\sqrt{\lambda^2\phi^2-(m\pi)^2} \quad ,(1/\phi)\sqrt{(m\pi)^2-\lambda^2\phi^2} \tag{3.69}$$

The solution to the building block 5 is extracted from the solution to building block 3 by replacing η with $1-\eta$. The solution to building block 6 is extracted from the building block 4 by replacing ξ with $1-\xi$.

$$W_5(\xi,\eta)=\sum_{m=0,1}^{K^*} E_m\left\{\theta_{11m}\frac{\cosh\beta_m(1-\eta)}{\sinh\beta_m}+\theta_{13m}\frac{\cos\gamma_m(1-\eta)}{\sin\gamma_m}\right\}\cos m\pi\xi$$
$$+\sum_{K^*+1}^{\infty} E_m\left\{\theta_{22m}\frac{\cosh\beta_m(1-\eta)}{\sinh\beta_m}+\theta_{23m}\frac{\cosh\gamma_m(1-\eta)}{\sinh\gamma_m}\right\}\cos m\pi\xi \tag{3.70}$$

where θ_{11m}, θ_{13m}, θ_{22m}, θ_{23m}, are as defined in equations 3.56, 3.57, 3.58 and 3.59 respectively.

$$W_6(\xi,\eta)=\sum_{m=0,1}^{K^*} E_m\left\{\theta_{11m}\frac{\cosh\beta_m(1-\xi)}{\sinh\beta_m}+\theta_{13m}\frac{\cos\gamma_m(1-\xi)}{\sin\gamma_m}\right\}\cos m\pi\eta$$
$$+\sum_{K^*+1}^{\infty} E_m\left\{\theta_{22m}\frac{\cosh\beta_m(1-\xi)}{\sinh\beta_m}+\theta_{23m}\frac{\cosh\gamma_m(1-\xi)}{\sinh\gamma_m}\right\}\cos m\pi\eta \tag{3.71}$$

where θ_{11m}, θ_{13m}, θ_{22m}, θ_{23m}, are as defined in equations 3.66, 3.67, 3.68 and 3.69 respectively.

3.2.3: Building Blocks 7 and 8

The solution to the building blocks 7 and 8 have already been developed as part

of the solution to the first building blocks. Following the same steps as for the first building block from equation 3.1 to 3.20, we obtain the solution for a building block with three slip shear edges and the edge $\eta=1$ having zero moment and a concentrated force, P_1 [13], at the point $\xi=\zeta$.

$$W(\xi,\eta)=P_1\sum_{m=0,1}^{K^*}\frac{-2}{\delta_m}\frac{\cos\ m\pi\zeta}{\theta_{11m}}[\cosh\ \beta_m\eta+\theta_{1m}\cos\ \gamma_m\eta] \\ +P_1\sum_{m=K^*+1}^{\infty}\frac{-2}{\delta_m}\frac{\cos\ m\pi\zeta}{\theta_{22m}}[\cosh\ \beta_m\eta+\theta_{2m}\cosh\ \gamma_m\eta] \tag{3.72}$$

where,

$$\theta_{1m}=\frac{(\beta_m^2-\nu\phi^2(m\pi)^2)\ \cosh\beta_m}{(\gamma_m^2+\nu\phi^2(m\pi)^2)\cos\gamma_m} \tag{3.73}$$

$$\theta_{2m}=\frac{(\beta_m^2-\nu\phi^2(m\pi)^2)\ \cosh\beta_m}{-(\gamma_m^2+\nu\phi^2(m\pi)^2)\cosh\gamma_m} \tag{3.74}$$

$$\theta_{11m}=\sinh\ \beta_m\ (\beta_m^3-(m\pi)^2\nu^*\phi\beta_m)+\sin\ \gamma\ (\theta_{1m}\gamma_m^3+(m\pi)^2\nu^*\theta_{1m}\gamma_m) \tag{3.75}$$

$$\theta_{22m}=\sinh\ \beta_m\ (\beta_m^3-(m\pi)^2\nu^*\phi\beta_m)+\sinh\ \gamma\ (\theta_{2m}\gamma_m^3-(m\pi)^2\nu^*\theta_{2m}\gamma_m) \tag{3.76}$$

For building block 7, we let $\zeta=0$. For building block 8, we let $\zeta=\alpha$.

$$W_7(\xi,\eta)=P_1\sum_{m=0,1}^{K^*}\frac{-2}{\delta_m\theta_{11m}}[\cosh\beta_m\eta+\theta_{1m}\cos\gamma_m\eta]\cos m\pi\xi$$
$$+P_1\sum_{m=K^*+1}^{\infty}\frac{-2}{\delta_m\theta_{22m}}[\cosh\beta_m\eta+\theta_{2m}\cosh\gamma_m\eta]\cos m\pi\xi \qquad (3.77)$$

$$W_8(\xi,\eta)=P_2\sum_{m=0,1}^{K^*}\frac{-2}{\delta_m}\frac{\cos m\pi\alpha}{\theta_{11m}}[\cosh\beta_m\eta+\theta_{1m}\cos\gamma_m\eta]\cos m\pi\xi$$
$$+P_2\sum_{m=K^*+1}^{\infty}\frac{-2}{\delta_m}\frac{\cos m\pi\alpha}{\theta_{22m}}[\cosh\beta_m\eta+\theta_{2m}\cosh\gamma_m\eta]\cos m\pi\xi \qquad (3.78)$$

3.3: The Eigenvalue Matrix

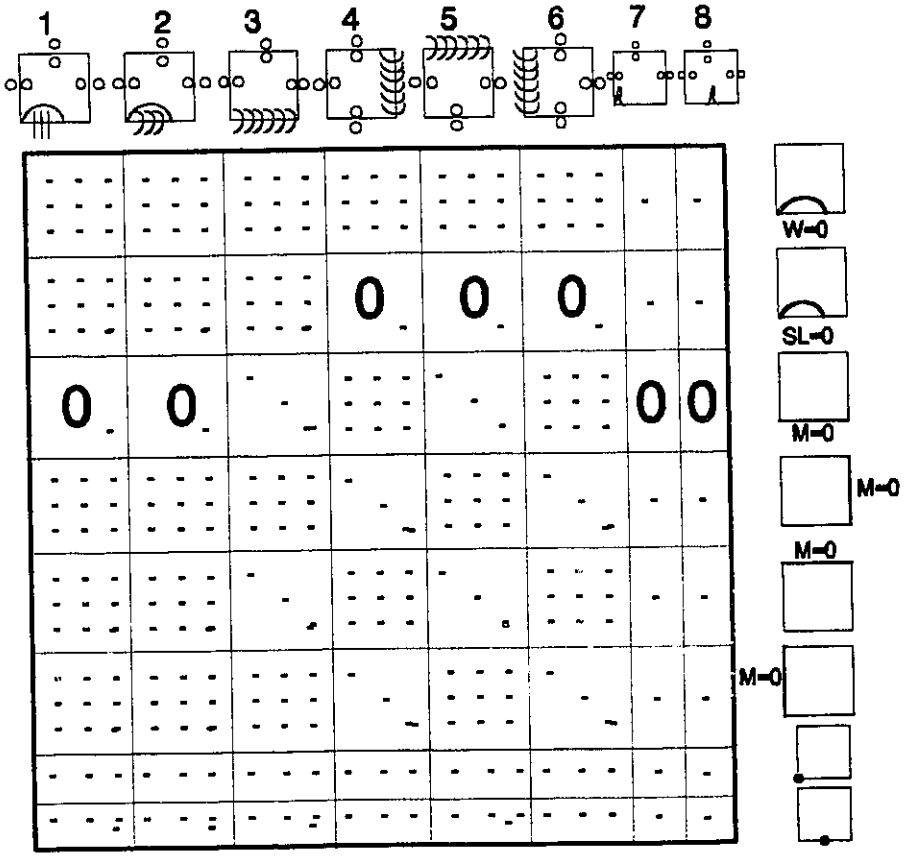

Figure3.8: A Schematic View of the Eigenvalue Matrix

Having solved every building block in the form of a cosine series it is now

necessary to adjust the coefficients of the series so that the sum of all the solutions satisfies the boundary conditions of the partially clamped cantilever plate.

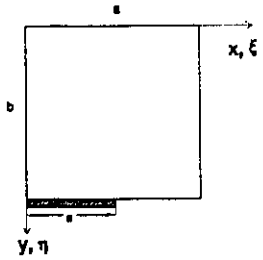

Figure3.9: The Partially Clamped Cantilever Plate

Before proceeding with a detailed mathematical development of the eigenvalue matrix, a brief qualitative explanation will be provided. Consider again the partially clamped cantilever plate shown in Figure 3.9. It has free conditions everywhere except at η=1 form $0 \leq \xi \leq \alpha$. where it is clamped. Referring now to the upper edge, η=0. It can be seen that none of the building blocks 1 to 8 contribute any vertical edge reaction. This condition is thus automatically satisfied. The other condition left to be satisfied on this edge is the condition of zero moment. All of the eight building blocks contribute moment so the coefficients must be adjusted so that the net contribution to moment is zero.

Figure 3.8 is a schematic representation of the eigenvalue matrix divided into 8x8 sections. The sixth row corresponds with the contributions of each building block to the moment along the upper edge. The moment contributions are of each building block are expanded as a cosine series and each net coefficient is set equal to zero. If each series is expanded to K terms then there will be 6K+2 coefficients and K homogeneous

algebraic equations in this portion of the matrix. Each section of the matrix is developed in a similar manner. It may be summarized as follows.

1. In the first set the net contribution to displacement in the region $0 \leq \xi \leq \alpha$ is expanded in a cosine series.
2. The second set pertains to slope in the region $0 \leq \xi \leq \alpha$.
3. The third set assures net contribution to moment along the cantilever edge of blocks 3 to 6 is zero.
4. The next three equation sets ensure zero moment along the other edges.
5. Sections 7 and 8 are used to enforce zero net lateral displacement at the extremities of the clamped region. They provide concentrated edge forces resulting from discontinuities in twisting moment at the clamped extremities.

Contibutions to the various boundary conditions are expanded as a cosine series. The sum of all the contributions must be zero. In order for the sum of orthogonal functions to equal zero, each net coefficient must equal zero. The entire matrix will have (6K+2)x(6K+2) elements resulting from (6K+2) homogeneous algebraic equations with (6K+2) coefficients each.

The shaded portion of the matrix in Figure 3.10 corresponds to the completely free plate and has been solved already in reference [13].

3.3.1: Building Block 1

The contributions of building block 1 correspond to the first column of the schematic matrix shown in Figure 3.8. To find the contributions of building block 1 to the displacement at $\eta=1$, $0 \leq \xi \leq \alpha$ expand the displacement given in equation 27 as a cosine

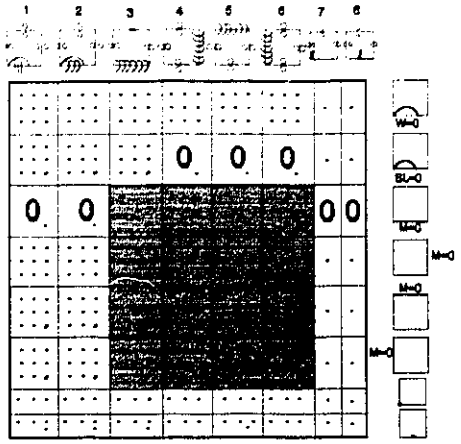

Figure3.10: Matrix Elements corresponding to the Completely Free Plate

series.

$$W_1(\xi,1)=\sum_{n=0,1}^{\infty} A_n \cos\frac{n\pi\xi}{\alpha} \tag{3.79}$$

The coefficient A_n is found by Fourier series theory,

$$A_n=\frac{2}{\alpha}\int_0^{\alpha} W_1(\xi,1)\cos\frac{n\pi\xi}{\alpha}d\xi \tag{3.80}$$

Substituting the solution thus far, for $W_1(\xi,\eta)$ and setting η=1 gives

$$\begin{aligned} A_n=&\frac{2}{\alpha}\sum_{m=0,1}^{K^*}\frac{-2}{\delta_m}\sum_{j=0,1}^{\infty}\frac{E_j}{\theta_{11m}}\phi_{jm}(\cosh\beta_m+\theta_{1m}\cos\gamma_m)\int_0^{\alpha}\cos m\pi\xi\cos\frac{n\pi\xi}{\alpha}d\xi \\ &+\frac{2}{\alpha}\sum_{K^*+1}^{\infty}\frac{-2}{\delta_m}\sum_{j=0,1}^{\infty}\frac{E_j}{\theta_{22m}}\phi_{jm}(\cosh\beta_m+\theta_{2m}\cosh\gamma_m)\int_0^{\alpha}\cos m\pi\xi\cos\frac{n\pi\xi}{\alpha}d\xi \end{aligned} \tag{3.81}$$

For an eigenvalue matrix M(6K+2, 6K+2), the element M(n,,j) for n, j=1 to K

$$M(n,j)=\frac{2}{\alpha}\sum_{m=0,1}^{K^*}\frac{-2}{\delta_m\theta_{11m}}\phi_{jm}(\cosh\beta_m+\theta_{1m}\cos\gamma_m)\int_0^{\alpha}\cos m\pi\xi\cos\frac{n\pi\xi}{\alpha}d\xi$$
$$+\frac{2}{\alpha}\sum_{K^*+1}^{KL}\frac{-2}{\delta_m\theta_{22m}}\phi_{jm}(\cosh\beta_m+\theta_{2m}\cosh\gamma_m)\int_0^{\alpha}\cos m\pi\xi\cos\frac{n\pi\xi}{\alpha}d\xi \quad (3.82)$$

To find the contributions of building block 1 to the slope at $\eta=1$, $0\le\xi\le\alpha$ expand the slope as a cosine series.

$$\frac{\partial W_1(\xi,1)}{\partial\eta}=\sum_{n=0,1}^{\infty}A_n\cos\frac{n\pi\xi}{\alpha} \quad (3.83)$$

The matrix elements are,

$$M(n+k,j)=\frac{2}{\alpha}\sum_{m=0,1}^{K^*}\frac{-2}{\delta_m\theta_{11m}}\phi_{jm}(\beta_m\cosh\beta_m-\theta_{1m}\gamma_m\cos\gamma_m)\int_0^{\alpha}\cos m\pi\xi\cos\frac{n\pi\xi}{\alpha}d\xi$$
$$+\frac{2}{\alpha}\sum_{K^*+1}^{KL}\frac{-2}{\delta_m\theta_{22m}}\phi_{jm}(\beta_m\cosh\beta_m+\theta_{2m}\gamma_m\cosh\gamma_m)\int_0^{\alpha}\cos m\pi\xi\cos\frac{n\pi\xi}{\alpha}d\xi \quad (3.84)$$

The contribution of building block 1 to the moment at $\eta=1$, is set equal to zero.

$$M(n+2K,j)=0 \quad (3.85)$$

3.3.2: Building Block 2

Expand as a cosine series, the displacement W_2 given in equation 48, at $\eta=1$, $0\le\xi\le1$.

$$W_2(\xi,1)=\sum_{n=0,1}^{\infty} A_n \cos\frac{n\pi\xi}{\alpha} \tag{3.86}$$

The procedure is the same as for building block 1, giving

$$\begin{aligned} M(n,j+K)=&\frac{2}{\alpha}\sum_{m=0,1}^{K^*}\frac{-2}{\delta_m\theta_{11m}}\phi_{jm}(\cosh\beta_m+\theta_{1m}\cos\gamma_m)\int_0^{\alpha}\cos m\pi\xi\cos\frac{n\pi\xi}{\alpha}d\xi \\ &+\frac{2}{\alpha}\sum_{K^*+1}^{KL}\frac{-2}{\delta_m\theta_{22m}}\phi_{jm}(\cosh\beta_m+\theta_{2m}\cosh\gamma_m)\int_0^{\alpha}\cos m\pi\xi\cos\frac{n\pi\xi}{\alpha}d\xi \end{aligned} \tag{3.87}$$

The constants here are defined as they are for W_2.

To find the contributions of building block 2 to the slope at $\eta=1$, $0\le\xi\le\alpha$ expand the slope a cosine series.

$$\frac{\partial W_2(\xi,1)}{\partial\eta}=\sum_{n=0,1}^{\infty} A_n \cos\frac{n\pi\xi}{\alpha} \tag{3.88}$$

The matrix elements are,

$$\begin{aligned} M(n+K,j+K)=&\frac{2}{\alpha}\sum_{m=0,1}^{K^*}\frac{-2}{\delta_m\theta_{11m}}\phi_{jm}(\beta_m\cosh\beta_m-\theta_{1m}\gamma_m\cos\gamma_m)\int_0^{\alpha}\cos m\pi\xi\cos\frac{n\pi\xi}{\alpha}d\xi \\ &+\frac{2}{\alpha}\sum_{K^*+1}^{KL}\frac{-2}{\delta_m\theta_{22m}}\phi_{jm}(\beta_m\cosh\beta_m+\theta_{2m}\gamma_m\cosh\gamma_m)\int_0^{\alpha}\cos m\pi\xi\cos\frac{n\pi\xi}{\alpha}d\xi \end{aligned} \tag{3.89}$$

The contribution of building block 2 to the moment at $\eta=1$, is set equal to zero.

$$M(n+2K,j+K)=0 \tag{3.90}$$

3.3.3: Building Block 3

Expand as a cosine series, the displacement W_2 given in equation 3.61, at $\eta=1$, $0\le\xi\le1$.

$$W_3(\xi,1)=\sum_{n=0,1}^{\infty} A_n \cos\frac{n\pi\xi}{\alpha} \tag{3.91}$$

Using Fourier series theory,

$$\begin{aligned} A_n=\frac{2}{\alpha}\sum_{m=0,1}^{K^*} E_m\left\{\theta_{11m}\frac{\cosh\beta_m}{\sinh\beta_m}+\theta_{13m}\frac{\cos\gamma_m}{\sin\gamma_m}\right\}\int_0^{\alpha}\cos m\pi\xi\frac{\cos n\pi\xi}{\alpha}d\xi \\ +\frac{2}{\alpha}\sum_{K^*+1}^{\infty} E_m\left\{\theta_{22m}\frac{\cosh\beta_m}{\sinh\beta_m}+\theta_{23m}\frac{\cosh\gamma_m}{\sinh\gamma_m}\right\}\int_0^{\alpha}\cos m\pi\xi\frac{\cos n\pi\xi}{\alpha}d\xi \end{aligned} \tag{3.92}$$

Therefore,

$$\begin{aligned} M(n,m+2K)=\frac{2}{\alpha}\left\{\theta_{11m}\frac{\cosh\beta_m}{\sinh\beta_m}+\theta_{13m}\frac{\cos\gamma_m}{\sin\gamma_m}\right\}\int_0^{\alpha}\cos m\pi\xi\frac{\cos n\pi\xi}{\alpha}d\xi \\ \frac{2}{\alpha}\left\{\theta_{22m}\frac{\cosh\beta_m}{\sinh\beta_m}+\theta_{23m}\frac{\cosh\gamma_m}{\sinh\gamma_m}\right\}\int_0^{\alpha}\cos m\pi\xi\frac{\cos n\pi\xi}{\alpha}d\xi \end{aligned} \tag{3.93}$$

3.3.4: Building Block 4

$$W_4(\xi,1)=\sum_{n=0,1}^{\infty} A_n \cos\frac{n\pi\xi}{\alpha} \tag{3.94}$$

$$A_n = \sum_{m=0,1}^{K^*} E_m \cos m\pi \int_0^{\alpha} \left\{ \theta_{11m} \frac{\cosh \beta_m \xi}{\sinh \beta_m} + \theta_{13m} \frac{\cos \gamma_m \xi}{\sin \gamma_m} \right\} \cos \frac{n\pi \xi}{\alpha} d\xi$$
$$+ \sum_{K^*+1}^{\infty} E_m \cos m\pi \int_0^{\alpha} \left\{ \theta_{22m} \frac{\cosh \beta_m \xi}{\sinh \beta_m} + \theta_{23m} \frac{\cos \gamma_m \xi}{\sinh \gamma_m} \right\} \cos \frac{n\pi \xi}{\alpha} d\xi \qquad (3.95)$$

Matrix elements are therefore,

$$M(m,n+4K) = \frac{2}{\alpha} \left\{ \frac{\theta_{11m}}{\sinh \beta_m} + \frac{\theta_{13m}}{\sin \gamma_m} \right\} \int_0^{\alpha} \cos m\pi \xi \cos \frac{m\pi \xi}{\alpha} d\xi$$
$$\frac{2}{\alpha} \left\{ \frac{\theta_{22m}}{\sinh \beta_m} + \frac{\theta_{23m}}{\sinh \gamma_m} \right\} \int_0^{\alpha} \cos m\pi \xi \cos \frac{m\pi \xi}{\alpha} d\xi$$

$$M(m,n+3K) = \frac{2}{\alpha} \cos m\pi \int_0^{\alpha} \left\{ \theta_{11m} \frac{\cosh \beta_m \xi}{\sinh \beta_m} + \theta_{13m} \frac{\cos \gamma_m \xi}{\sin \gamma_m} \right\} \cos \frac{n\pi \xi}{\alpha} d\xi$$
$$\frac{2}{\alpha} \cos m\pi \int_0^{\alpha} \left\{ \theta_{22m} \frac{\cosh \beta_m \xi}{\sinh \beta_m} + \theta_{23m} \frac{\cosh \gamma_m \xi}{\sinh \gamma_m} \right\} \cos \frac{n\pi \xi}{\alpha} d\xi \qquad (3.97)$$

3.3.5: Building Block 5

Using the same procedure as above we get,

$$M(m,n+4K) = \frac{2}{\alpha} \left\{ \frac{\theta_{11m}}{\sinh \beta_m} + \frac{\theta_{13m}}{\sin \gamma_m} \right\} \int_0^{\alpha} \cos m\pi \xi \cos \frac{m\pi \xi}{\alpha} d\xi \quad (\lambda^2 < (m\pi)^2)$$
$$\frac{2}{\alpha} \left\{ \frac{\theta_{22m}}{\sinh \beta_m} + \frac{\theta_{23m}}{\sinh \gamma_m} \right\} \int_0^{\alpha} \cos m\pi \xi \cos \frac{m\pi \xi}{\alpha} d\xi \quad (\lambda^2 < (m\pi)^2) \qquad (3.98)$$

3.3.6: Building Block 6

$$M(m,n+5K)=\frac{2}{\alpha}\cos m\pi\int_0^{\alpha}\left\{\theta_{11m}\frac{\cosh\beta_m(1-\xi)}{\sinh\beta_m}+\theta_{13m}\frac{\cos\gamma_m(1-\xi)}{\sin\gamma_m}\right\}\cos\frac{m\pi\xi}{\alpha}d\xi \qquad (3.99)$$

$$\frac{2}{\alpha}\cos m\pi\int_0^{\alpha}\left\{\theta_{22m}\frac{\cosh\beta_m(1-\xi)}{\sinh\beta_m}+\theta_{23m}\frac{\cosh\gamma_m(1-\xi)}{\sinh\gamma_m}\right\}\cosh\frac{m\pi\xi}{\alpha}d\xi$$

3.3.7: Building Block 7

$$M(m,6K+1)=\sum_{m=0,1}^{K^*}\frac{-2}{\delta_m\theta_{11m}}[\cosh\beta_m+\theta_{1m}\cos\gamma_m]\int_0^{\alpha}\cos m\pi\xi\cos\frac{m\pi\xi}{\alpha}d\xi \qquad (3.100)$$

$$+\sum_{m=K^*+1}^{KL}\frac{-2}{\delta_m\theta_{22m}}[\cosh\beta_m+\theta_{2m}\cosh\gamma_m]\int_0^{\alpha}\cos m\pi\xi\cos\frac{m\pi\xi}{\alpha}d\xi$$

3.3.8: Building Block 8

$$M(m,6K+2)=\sum_{m=0,1}^{K^*}\frac{-2\cos m\pi\alpha}{\delta_m\theta_{11m}}[\cosh\beta_m+\theta_{1m}\cos\gamma_m]\int_0^{\alpha}\cos m\pi\xi\cos\frac{m\pi\xi}{\alpha}d\xi \qquad (3.101)$$

$$+\sum_{m=K^*+1}^{KL}\frac{-2\cos m\pi\alpha}{\delta_m\theta_{22m}}[\cosh\beta_m+\theta_{2m}\cosh\gamma_m]\int_0^{\alpha}\cos m\pi\xi\cos\frac{m\pi\xi}{\alpha}d\xi$$

3.4: The Natural Frequencies

Having completely developed the eigenvalue matrix, the next step is to use it to find the natural frequencies, $f=\omega/2\pi$. Each element of the eigenvalue matrix is a function of the eigenvalue, $\lambda^2=(\omega(\rho/D)^{1/2})$. If there are non trivial solutions to the eigenvalue

matrix, then the determinent of the matrix must equal zero. Arbitrary values of λ^2 are entered into the program, the determinant is computed using standard techniques. If the determinant is not zero then λ^2 is incremented by a given amount Δ and the determinant is re-computed. The iteraction is continued until the determinant vanishes at which point λ^2 will be correct. To find the next mode eigenvalues, λ^2, is incremented until the determinant is again zero. This is repeated for every mode. This procedure may be described concisely in the following equations. The homogeneous set of algebraic equations is represented as,

$$[M(\omega)]\{X\}=\{0\} \tag{3.102}$$

The natural frequencies of the system are determined by solving

$$\det[M(\omega)]=0 \tag{3.103}$$

3.5: The Mode Shapes

Once the eigenvalue is found, the 6K+2 unknown coefficients are found by arbitrarily setting one of the unknowns equal to one and then solving for the remaining 6K+1 unknowns. The mode shapes are computed by simply summing the eight displacement functions given in section 3.2.

$$W(\xi,\eta)=W_1+W_2+W_3+W_4+W_5+W_6+W_7+W_8 \tag{3.104}$$

This function gives the displacement at any point, (ξ,η), of the plate. Any desired parameters, ϕ and α can be used.

Chapter 4: The Computing Method

A computer program was written to evaluate all the results from the solutions obtained. The program was written in FORTRAN and consists of approximately 1500 lines of source code. The program is a modification of another program written to solve the completely free plate problem (building blocks 3 to 6). The seventh and eighth building blocks have also been solved previously for other plate problems [12]. They were imported and adjusted appropriately. The first and second building block solutions are unique to this problem.

The program consists of a main part which generates the eigenvalue matrix, and several subroutines to compute the shape function, the determinant, the unknown coefficients, and various integrals. The structure of the program is summarised below.

Main Program

- Input variables, λ^2, Δ, α, K, KL, ϕ, ν
- Generate eigenvalue matrix using the equations given in section 3.3
- Call determinant subroutine
- Evaluate eigenvalue (call integral subroutines)
- Call subroutine to solve simultaneous equations
- Call shape subroutine
- Output shape and frequency data
- End

Subroutines

- Integrals
- Determinant
- Simultaneous Equations
- Shape

The program used works but there are ways in which the efficiency and clarity may be improved. This is discussed further in chapter 6.

Chapter 5: Results and Discussion

5.1: Convergence

Since the solution formulated here is in the form of an infinite series it is necessary to truncate the series in order to obtain results. It is essential to ensure that the series has not been truncated before the result has converged to the desired degree of accuracy. The solutions to the building blocks 1, 2, 7 and 8 are developed with Dirac delta functions so they contain series within a series. That is, each term in the series is itself a series. For this reason, two convergence tests must be done. It is necessary to have sufficient terms in both series. There are six convergence tests shown in Figures 5.2 to 5.7. They are the first mode eigenvalues for plates with aspect ratios of 1 and 2/3, and clamped lengths 25%, 50%, and 75% of the plate dimension. The y-axis shows the eigenvalues, λ^2, and the x-axis shows the number of terms, K, in the series. The various lines on each graph show the convergence of the Dirac delta function series. The lines of a higher number of terms, KL, are closer together and at convergence they overlap. The convergence is discussed for each case in the caption of the graphs.

It should be pointed out that the number of terms in the Dirac delta function series must be much greater then the number of terms in the solution series. This can be explained by again considering the edge $\eta=1$ of the cantilever plate. The Dirac delta functions are expanded over the entire length of the edge. The enveloping function, however, is expanded only in the region $0\leq\xi\leq\alpha$. Therefore, the enveloping function cannot represent the sum of the Dirac functions unless the Dirac functions have at least K/α terms. This is to ensure that the density of waves along the driven segment of the boundary does not exceed the density of waves in the same direction for the plate response [13]. This is easily demonstrated with a simple sine series,

$$f_1(x) = \sum_{m=1}^{K} A_m \sin\frac{m\pi x}{L} \quad , \quad f_2(x) = \sum_{m=1}^{KL} B_m \sin\frac{m\pi x2}{L}$$

Consider the first term of these two series, $f_1(x)$ expanded over length L, and $f_2(x)$ expanded over the length L/2 (see Figure 5.1). It is clear that $f_1(x)$ can never envelope $f_2(x)$ unless at least two terms of $f_2(x)$ are used. It is for this reason that as the clamped length decreases, the number of terms, KL, used in the Dirac delta function series must increase to allow a sufficiently large K for convergence. It can be noted from the graphs (Figure 5.2-5.4), that the K terms converge up and the KL terms converge down. That is, the eigenvalue increases with increasing K and it decreases with increasing KL.

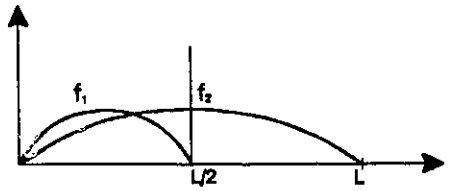

Figure 5.1: KL>K/α

Figure 5.2: Convergence to 3 digit accuracy at KL=70 and K=15

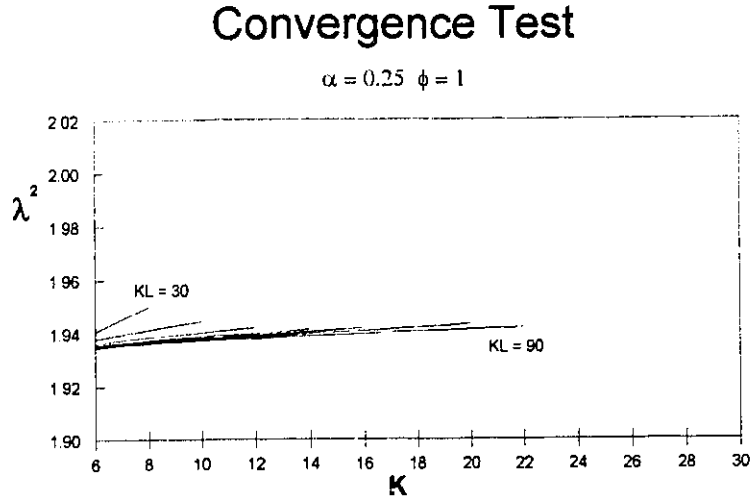

Figure 5.3: Convergence to 3 digit accuracy at KL=60 and K=14

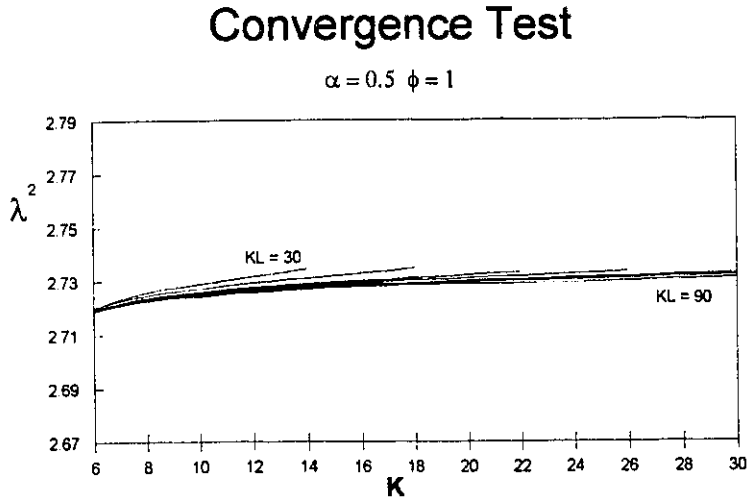

Figure 5.4: Convergence to 3 digit accuracy at KL=50 and K=10

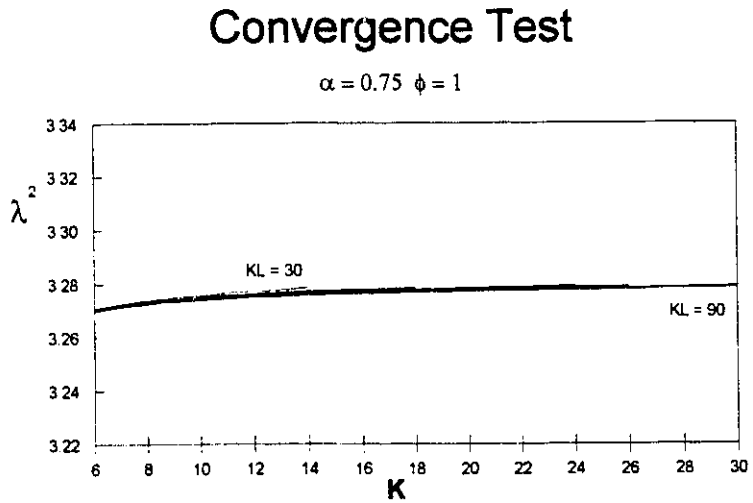

Figure 5.5: Convergence to 3 digit accuracy at KL=80 and K=18

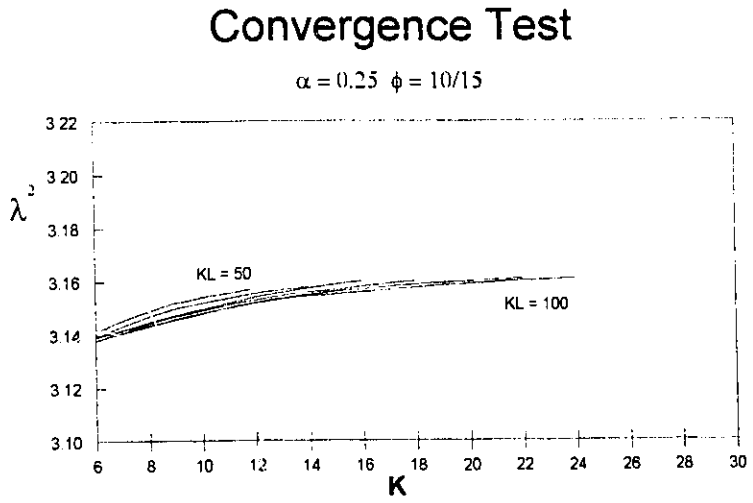

Figure 5.6: Convergence to 3 digit accuracy at KL=70 and K=24

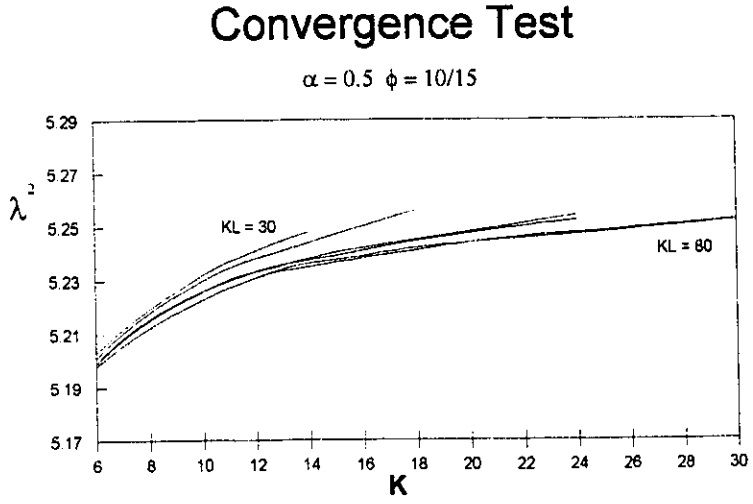

Figure 5.7: Convergence to 3 digit accuracy at KL=60 and K=18

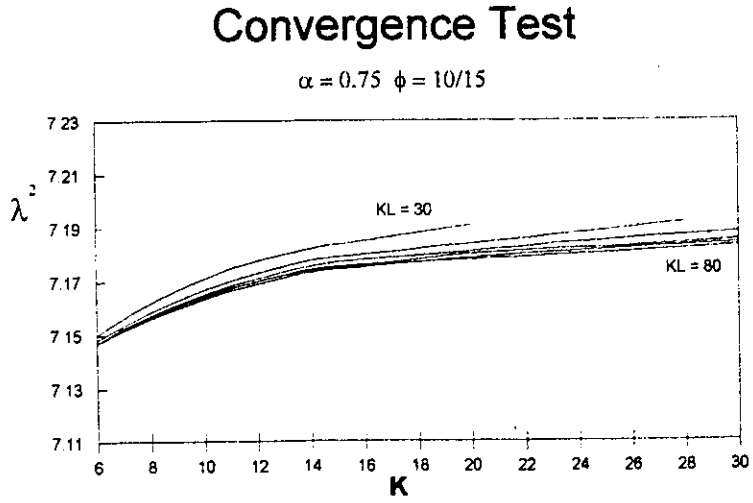

5.2: The Natural Frequencies

5.2.1: Validity

Experimental results were obtained from R.K. Singhal of the Canadian Space Agency. The experimental method used was impact testing. The apparatus is described in detail in reference [13]. Results for comparison were also obtained by running the commercial finite element method software package called ALGOR. A 20x20 mesh of rectangular elements was used.

Figure 5.8 compares the computed natural frequencies with the experimental results. Figure 5.9 compares the computed results with the FEM results (obtained by L.Caravaggio of SPAR Aerospace. The plate used for the comparison is aluminum ($E= 10x10^6$ lb/in^2, $\rho=9.75x10^{-2}$ lb/in^3, $\nu=.333$) with dimensions a=15in, b=10in and clamped half way across the edge. The thickness, h, used is .0625in. The results in both cases agree to within 3% confirming that the method is valid. The values are given in Table 5.1. Table 5.2 is another comparison of theoretical and experimental frequencies found for plates with an aspect ratio of 1. All other parameters are the same as above. The agreement is again very good. Another method to check the results is to let $\alpha=1$, giving regular cantilever plate conditions for which there are numerous published results. Comparisons are given in Table 5.4 for the plate of aspect ratio equal to one. Letting α approach zero will not correspond to the completely free condition because of the conditons imposed by the seventh and eighth building blocks.

Figure 5.8: Comparison of Experimental (obtained by R.K. Singhal of the Canadian Space Agency) and Analytical Frequencies

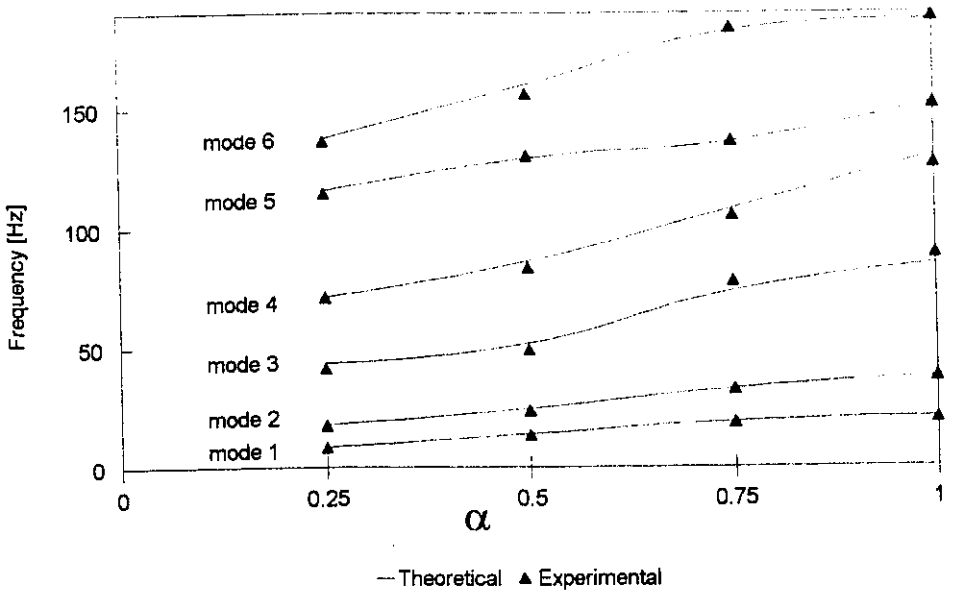

Figure 5.9: Comparison of FEM (obtained by L.Caravaggio of SPAR Aerospace) and Analytical Frequencies

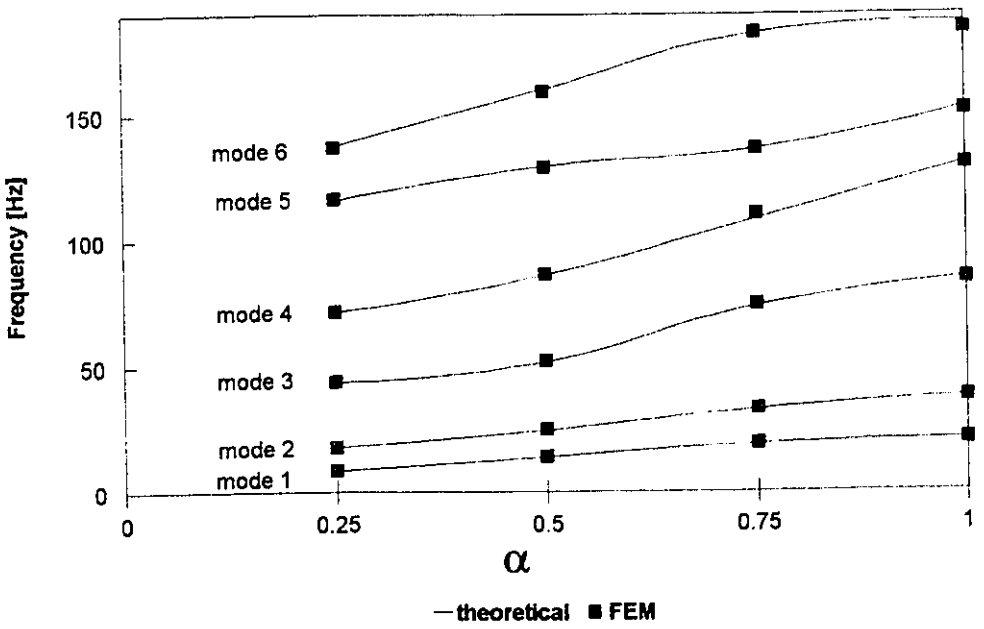

Table 5.1: Analytical, experimental and FEM resonant frequencies for a rectangular aluminum plate (10" x 15")

Mode	α= 0.25 [Hz]			α= 0.50 [Hz]			α= 0.75 [Hz]		
	analyt	exper	FEM	analyt	exper	FEM	analyt	exper	FEM
1	8.4	8.2	8.6	13.9	13.4	14.2	19.0	18.6	19.2
2	17.8	17.6	18.0	24.5	23.6	24.9	32.7	32.6	33.1
3	43.7	41.4	43.9	51.9	49.1	52.4	73.9	78.0	74.8
4	71.5	71.2	71.9	85.4	83.5	85.8	108.5	105.7	110.7
5	115.9	114.8	115.4	129.5	130.4	129.1	135.5	135.7	135.4
6	137.8	135.6	137.2	160.2	155.2	159.5	182.4	183.9	182.7

Table 5.2: Analytical, experimental and FEM resonant frequencies for a rectangular aluminum plate (10" x 10")

Mode	α= 0.25 [Hz]		α= 0.50 [Hz]		α= 0.75 [Hz]	
	analyt	exper	analyt	exper	analyt	exper
1	11.6	10.8	15.3	15.7	19.5	18.9
2	25.6	24.7	35.0	35.0	45.4	41.8
3	64.6	63.6	82.0	81.2	113.4	105.8
4	129.6	127.9	138.6	137.0	158.2	155.8
5	145.0	145.8	158.1	157.9	165.1	161.2
6	188.0	183.7	201.8	199.1	260.1	253.4

5.2.2: Results

The following tables show the first six mode eigenvalues computed for partially clamped cantilever plates with varying aspect ratios, ϕ, and varying clamped lengths, α.

Tables 5.3: Computed Eigenvalues, $\lambda^2=(\omega a^2(\rho/D)^{1/2})$, $\phi=2/3$, $\nu=0.333$

Mode	Clamped Length			
	$\alpha=0.25$	$\alpha=0.5$	$\alpha=0.75$	$\alpha=1.0$
1	3.16	5.24	7.17	7.81
2	6.72	9.25	12.3	14.2
3	15.5	19.6	27.9	32.0
4	27.0	32.6	40.9	49.2
5	43.7	48.9	51.5	57.6
6	52.0	60.5	68.8	70.4

Tables 5.4: Computed Eigenvalues, $\lambda^2= (\omega a^2(\rho/D)^{1/2})$, $\phi=1.0$, $\nu=0.333$

Mode	Clamped Length			
	$\alpha=0.25$	$\alpha=0.5$	$\alpha=0.75$	$\alpha=1.0$
1	1.94	2.73	3.28	3.46 (3.494)
2	4.29	6.03	7.62	8.36 (8.547)
3	10.8	13.8	19.0	21.1 (21.44)
4	21.7	23.3	25.5	27.1 (27.46)
5	24.5	25.5	27.9	30.5 (31.17)
6	31.5	33.9	43.6	53.5

( ) Leissa [4]

Tables 5.5: Computed Eigenvalues, $\lambda^2 = (\omega a^2(\rho/D)^{1/2})$, ϕ=1.5 , ν=0.333

Mode	Clamped Length			
	α=0.25	α=0.5	α=0.75	α=1.0
1	1.02	1.29	1.47	1.52
2	2.98	4.03	4.38	4.38
3	4.39	4.38	4.78	5.07
4	5.83	8.05	9.07	9.47
5	9.86	9.86	9.86	9.86
6	10.80	12.9	14.2	14.2

Tables 5.6: Computed Eigenvalues, $\lambda^2 = (\omega a^2(\rho/D)^{1/2})$, ϕ=2.0 , ν=0.333

Mode	Clamped Length			
	α=0.25	α=0.5	α=0.75	α=1.0
1	.62	0.75	0.831	0.85
2	2.30	2.46	2.46	2.46
3	2.46	3.03	3.46	3.62
4	4.43	4.83	5.17	5.32
5	7.33	9.34	11.23	14.93
6	12.33	12.34	12.33	19.73

Tables 5.7: Computed Eigenvalues, $\lambda^2 = (\omega a^2(\rho/D)^{1/2})$, ϕ=2.5, ν=0.333

Mode	Clamped Length			
	α=0.25	α=0.5	α=0.75	α=1.0
1	0.41	0.49	0.530	0.545
2	1.57	1.57	1.57	1.57
3	1.92	2.42	2.71	2.81
4	3.01	3.18	3.32	3.39
5	5.70	5.31	5.31	5.31
6	5.31	7.28	8.57	8.98

5.2.3: Trends

Some trends apparent when varying the clamped length are shown graphically for the first six modes in Figures 5.8 and 5.9. It is seen that as α increses the eigenvalue also increases. There is less variation in the eigenvalues as α is varied in the upper end of its range. Figures 5.10 and 5.11 show the eigenvalue variation with the aspect ratio, ϕ, for the first and second mode eigenvalues respectively. It is clear that the eigenvalues are sensitive to ϕ values below approximately 1.5. At values of ϕ greater than 1.5 the eigenvalues converge. Figures 5.10 and 5.11 also display the insensitivity to α of the eigenvalue at α>0.75 (the lines are close together).

Figure 5.10:

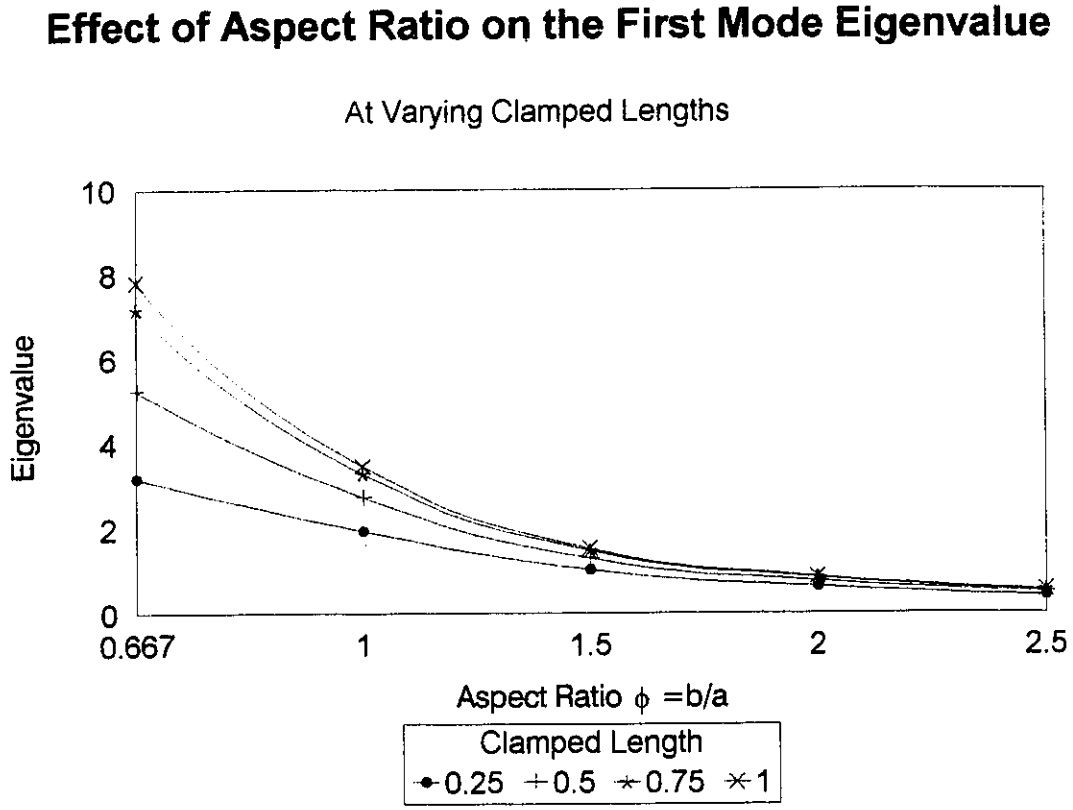

Figure 5.11:

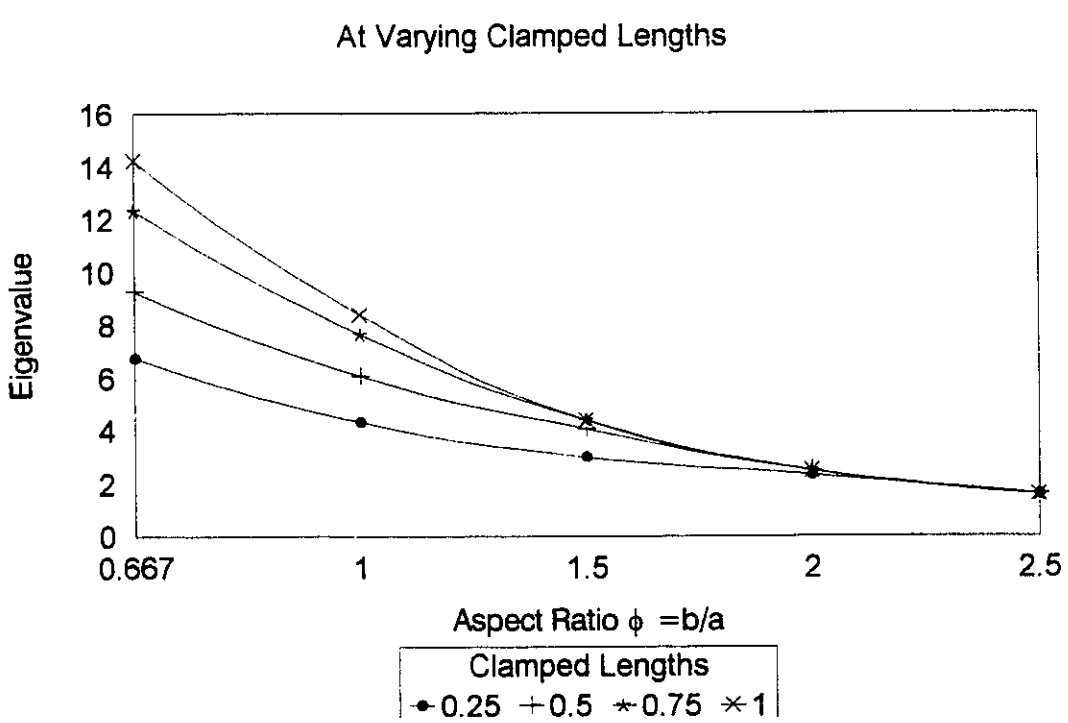

5.3: The Mode Shapes

5.3.1: Validity

Computed and experimental mode shapes for the first six modes are shown below, in Figures 5.10 to 5.15. The plate used for this comparison is the same as the one described on page 61 for comparing the natural frequencies. The plate shown are clamped in the region $(1-\alpha)\leq\xi\leq1$. It is shown this way for easy comparison with the experimental data which was provided in this format. The dashed line represents the plate with zero displacement. The agreement of the mode shapes found by experimental and analytical techniques is excellent.

5.3.1: Results

The first six mode shapes are shown below in Figures 5.18-53 for plates with an aspect ratio, $\phi=1$ and clamped lengths $\alpha=0.25$, $\alpha=0.5$ and $\alpha=0.75$. The shapes are shown both as mesh plots and contour diagrams.

5.3.2: Trends

It can be seen from the mesh plots that the conditions of zero slope and displacement are met in the clamped region of the plate. This is also evident from the contour diagrams as the lines of constant displacement move away from the clamped region. The plates with a greater clamped length have a larger area of very little displacement. The displacement nodes follow similar patterns but rotate in the counter clockwise direction as α increases. This is most clearly seen in the case of the first mode

which consists only of parallel lines but follows for the higher modes also on close inspection.

Analytical Mode Shapes

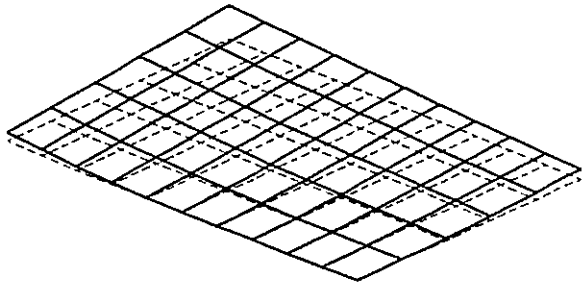

Figure 5.12: Mode 1

Experimental Mode Shapes

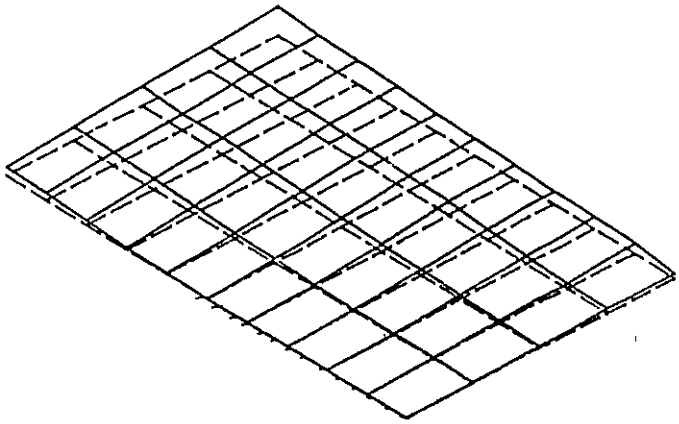

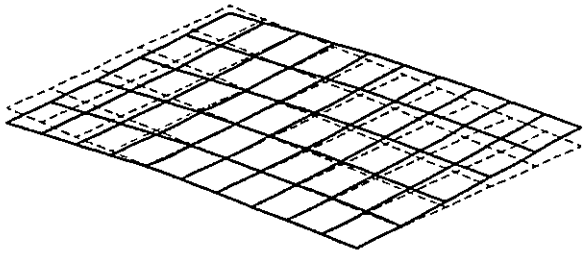

Figure 5.13: Mode 2

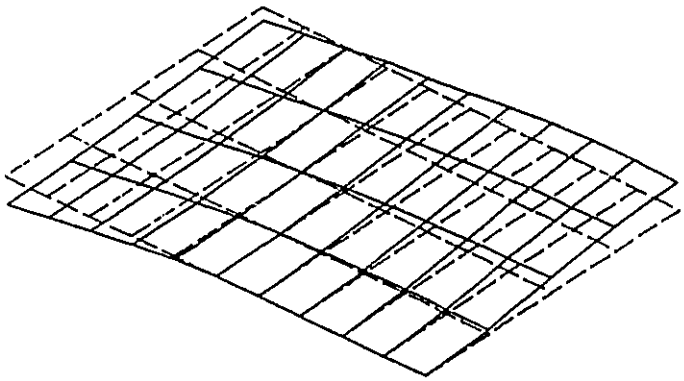

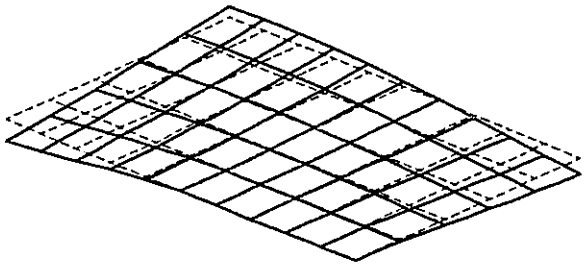

Figure 5.14: Mode 3

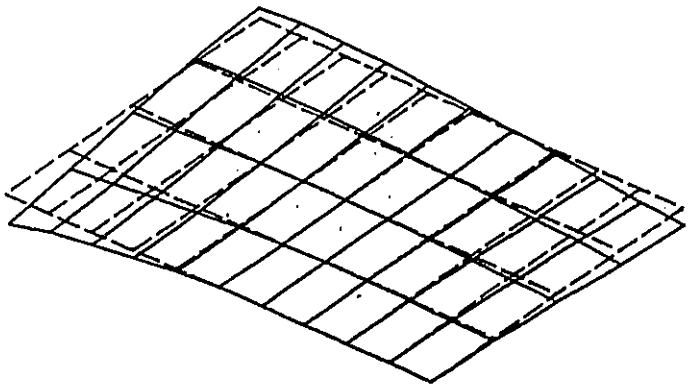

Analytical Mode Shapes

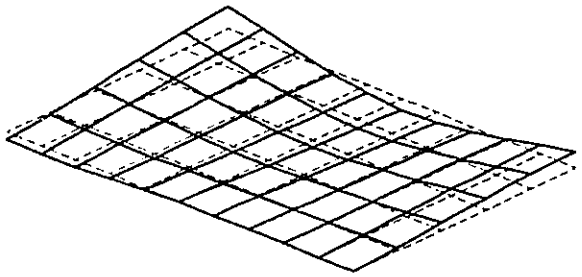

Figure 5.15: Mode 4

Experimental Mode Shapes

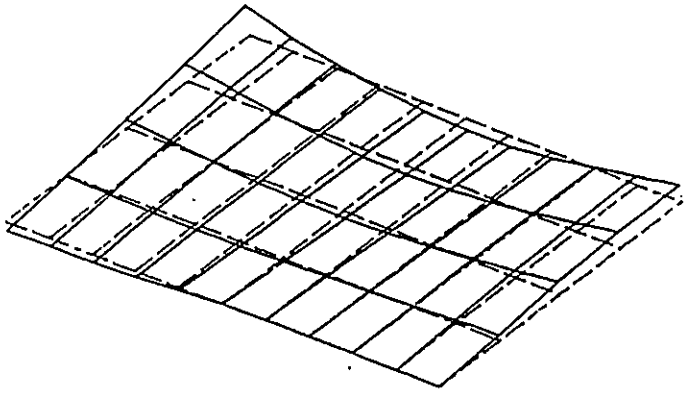

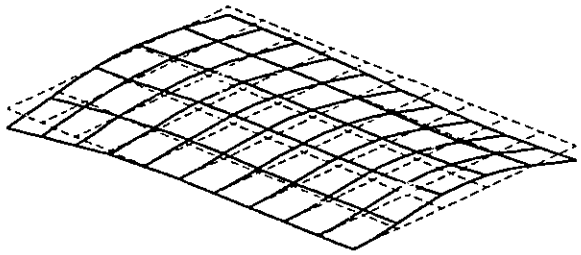

Figure 5.16: Mode 5

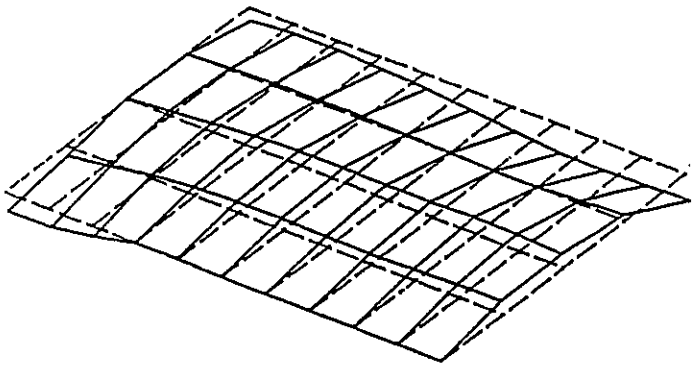

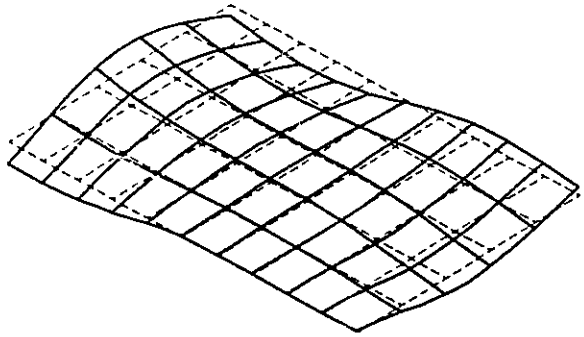

Figure 5.17: Mode 6

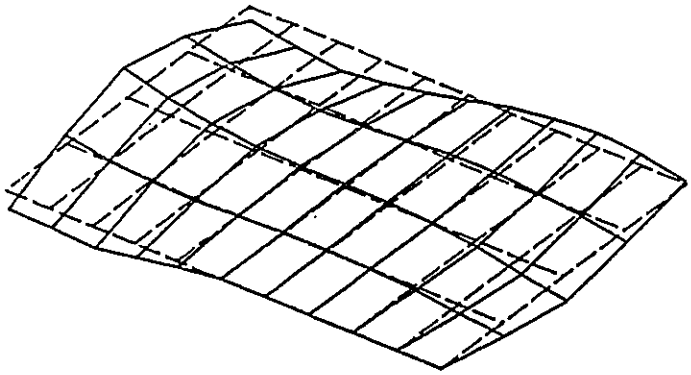

Mesh Plots of Computed Mode Shapes

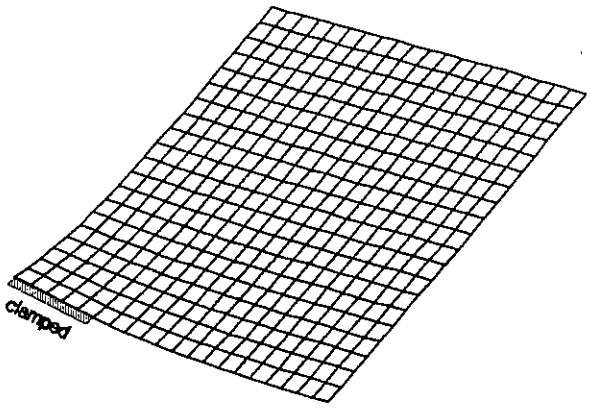

Figure 5.18: Mode 1, α=0.25

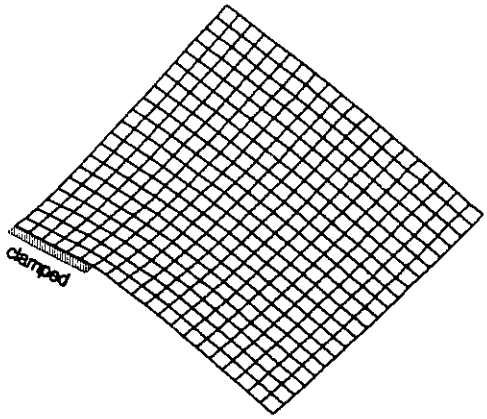

Figure 5.19: Mode 2, α=0.25

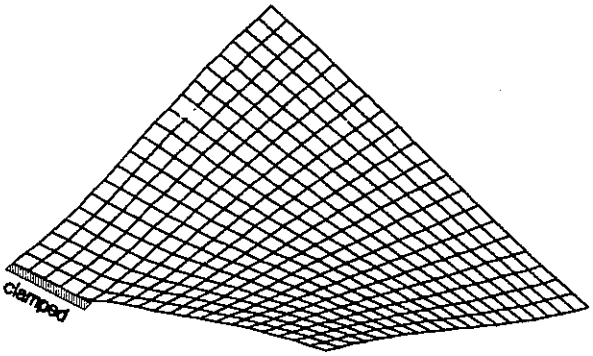

Figure 5.20: Mode 3, α=0.25

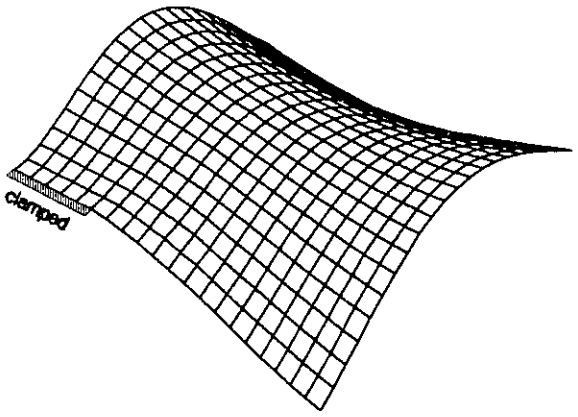

Figure 5.21: Mode 4, α=0.25

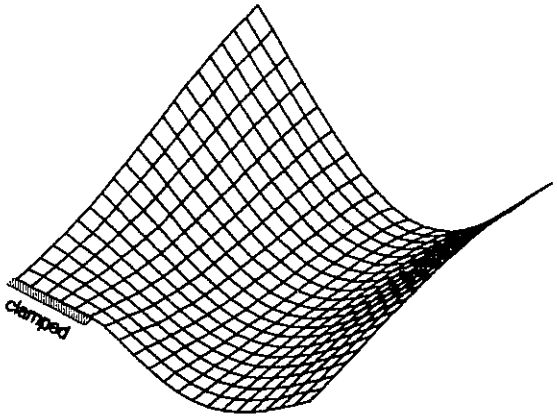

Figure 5.22: Mode 5, α=0.25

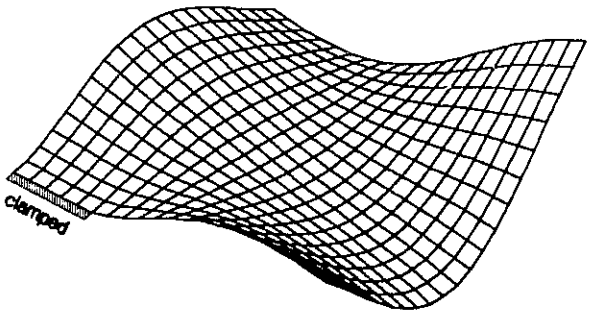

Figure 5.23: Mode 6, α=0.25

Contour Plots of the Computed Mode Shapes

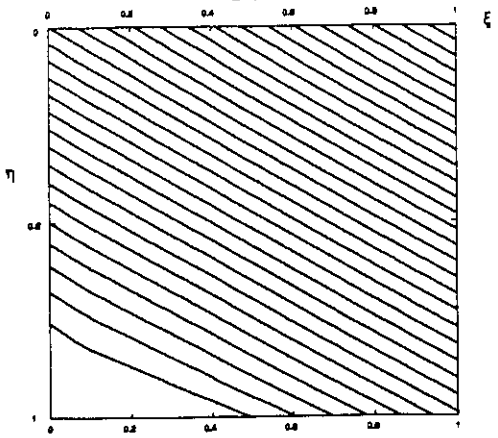

Figure 5.24: Mode 1, α=0.25

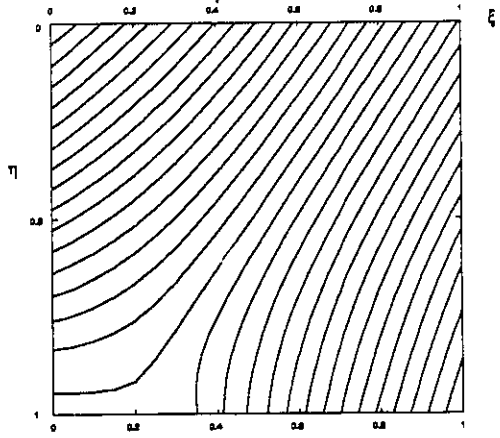

Figure 5.25: Mode 2, α=0.25

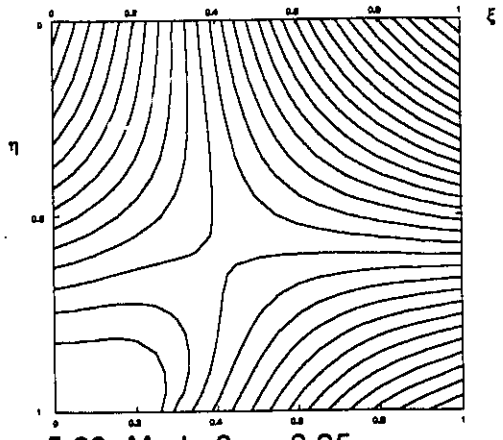

Figure 5.26: Mode 3, α=0.25

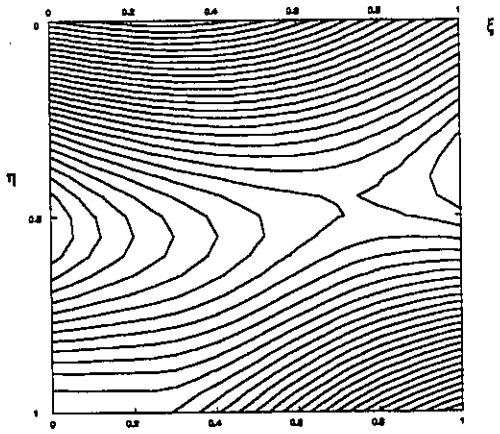

Figure 5.27: Mode 4, α=0.25

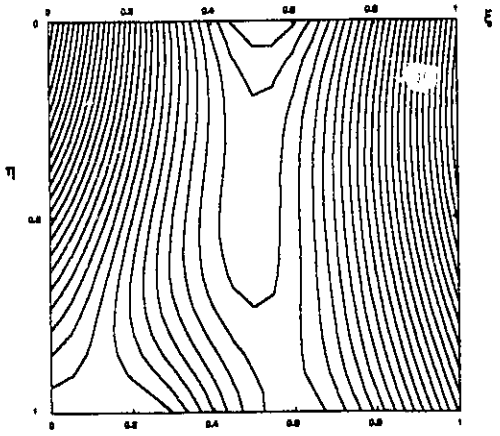

Figure 5.28: Mode 5, α=0.25

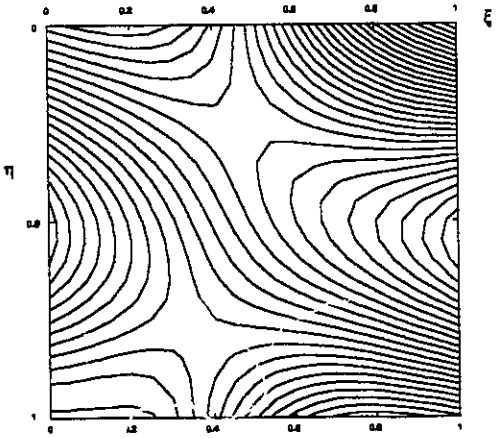

Figure 5.29: Mode 6, α=0.25

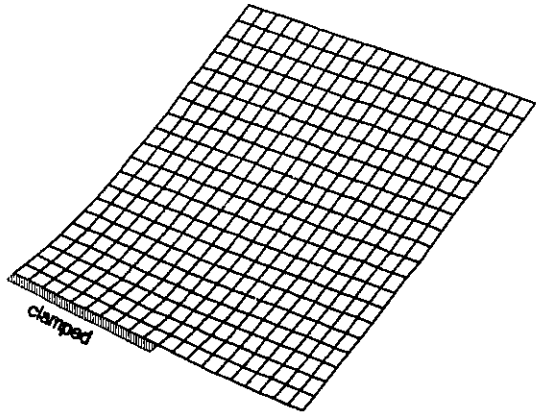

Figure 5.30: Mode 1, α=0.5

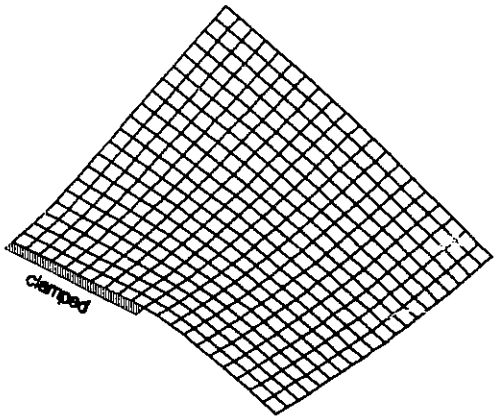

Figure 5.31: Mode 2, α=0.5

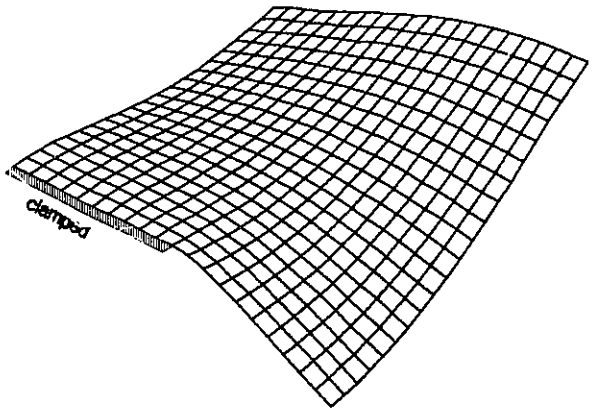

Figure 5.32: Mode 3, α=0.5

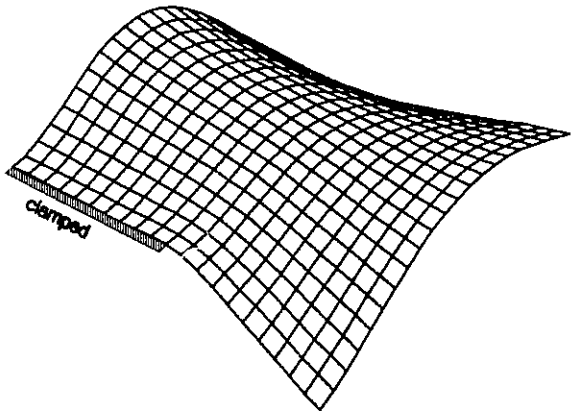

Figure 5.33: Mode 4, α=0.5

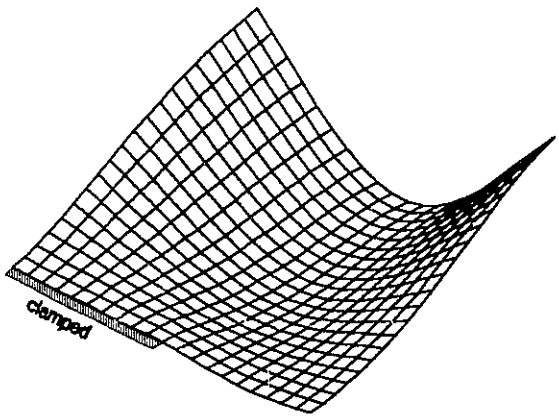

Figure 5.34: Mode 5, α=0.5

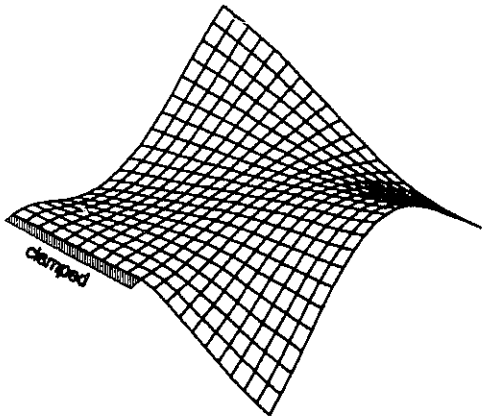

Figure 5.35: Mode 6, α=0.5

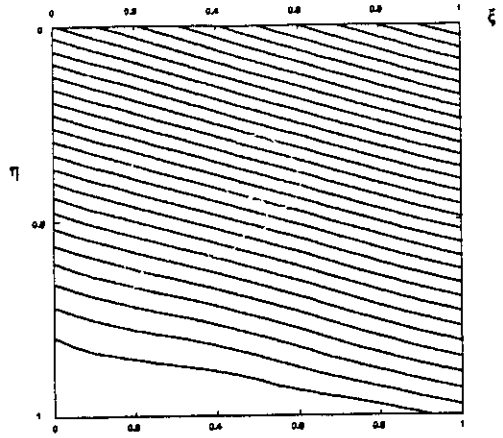

Figure 5.39: Mode 1, α=0.5

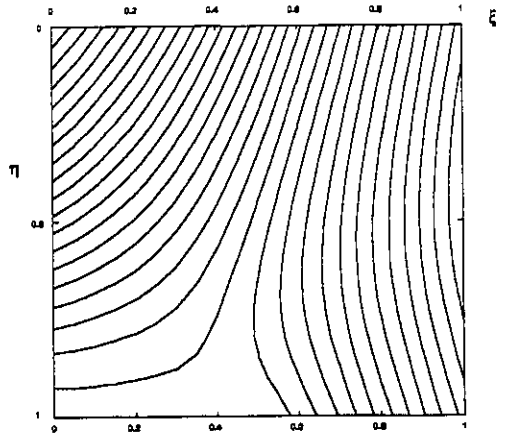

Figure 5.36: Mode 2, α=0.5

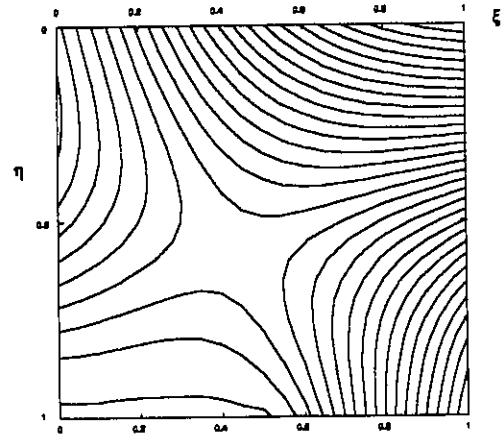

Figure 5.37: Mode 3, α=0.5

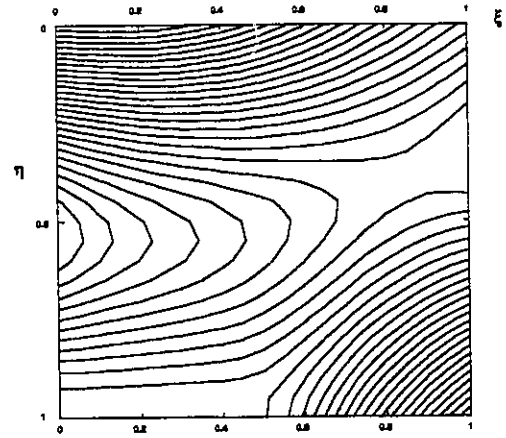

Figure 5.38: Mode 4, α=0.5

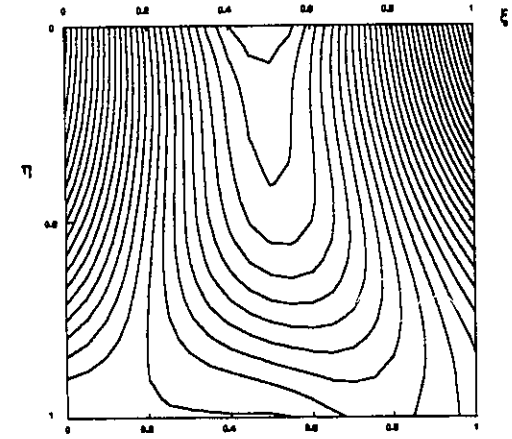

Figure 5.40: Mode 5, α=0.5

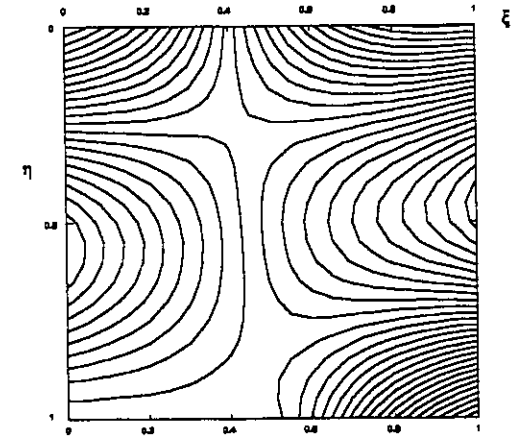

Figure 5.41: Mode 6, α=0.5

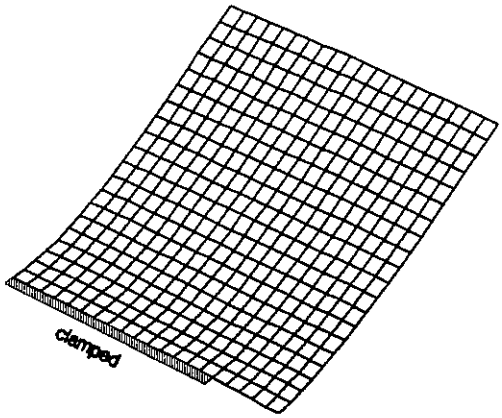

Figure 5.42: Mode 1, α=0.75

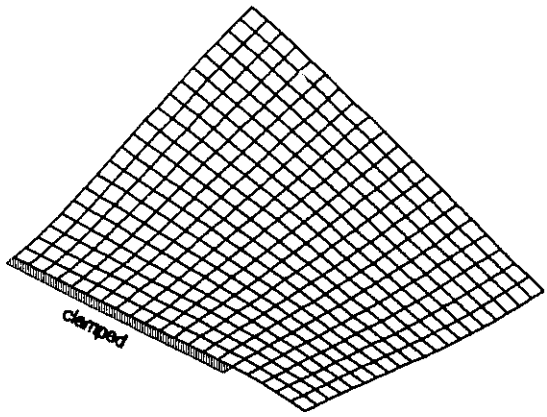

Figure 5.43: Mode 2, α=0.75

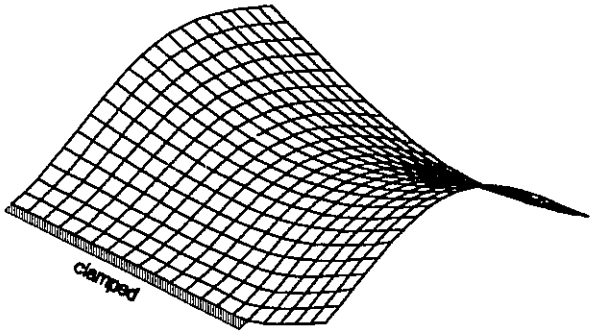

Figure 5.44: Mode 3, α=0.75

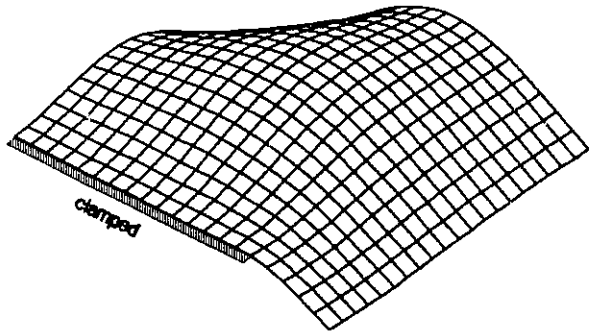

Figure 5.45: Mode 4, α=0.75

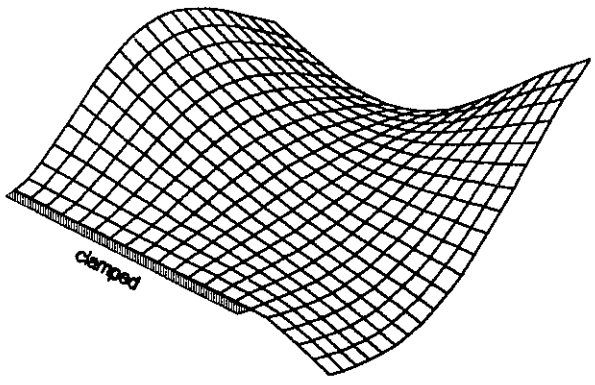

Figure 5.46: Mode 5, α=0.75

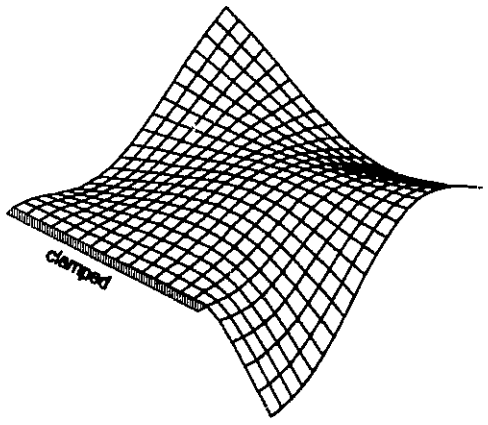

Figure 5.47: Mode 6, α=0.75

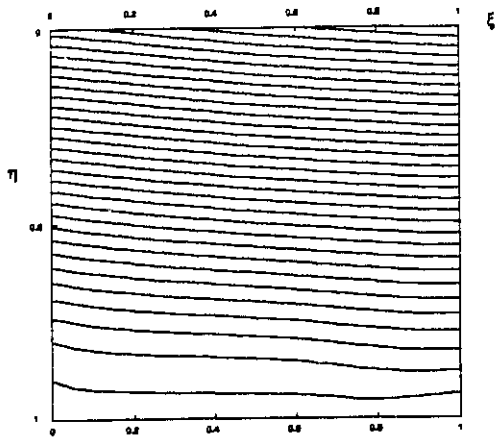

Figure 5.48: Mode 1, α=0.75

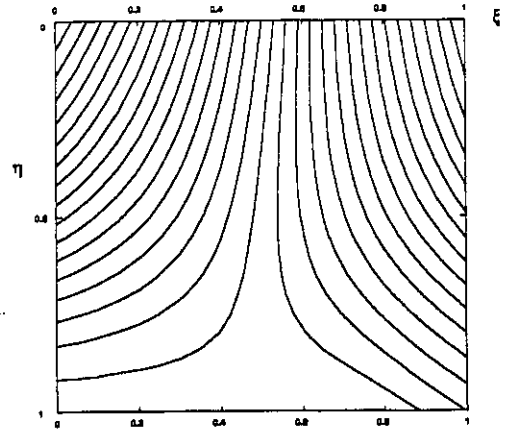

Figure 5.49: Mode 2, α=0.75

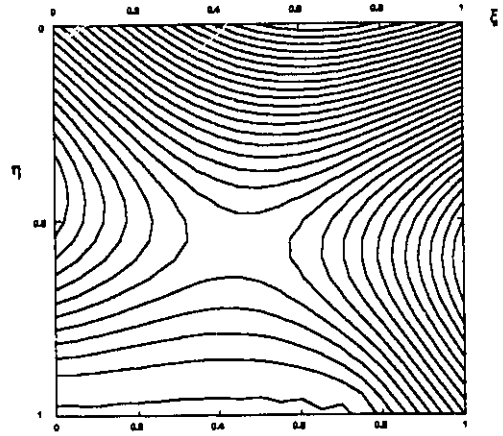

Figure 5.50: Mode 3, α=0.75

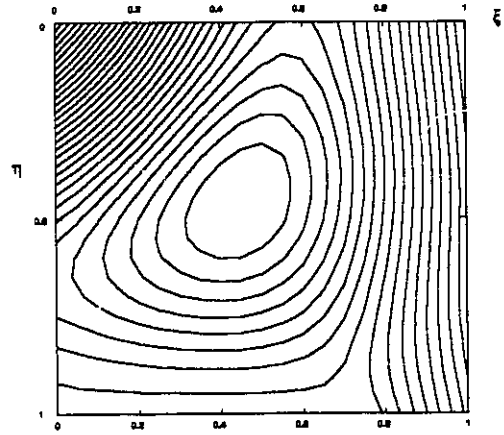

Figure 5.51: Mode 4, α=0.75

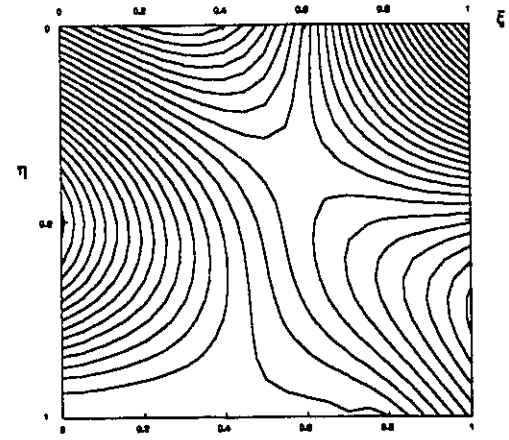

Figure 5.52: Mode 5, α=0.75

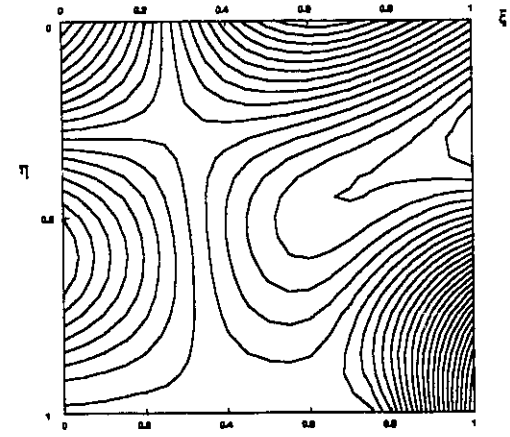

Figure 5.53: Mode 6, α=0.75

Chapter 6: Further Research Possibilities and Conclusions

6.1: Elastically Restrained Edge

A logical extension of the work provided here would be to formulate the solution to allow for a finite stiffness in the partially clamped region. This would be a more accurate model of the actual situation of the circuit board supports. The modifications necessary to the above formulated solution would be minimal since only the second building block contributes moment to the supported region. For an edge support with a spring constant k the moment is

$$M_y = k\frac{dw}{dy}$$

In dimensionless form this may be expressed as [15]

$$\frac{Mb^2}{aD} = \frac{kb}{D}\frac{\partial W}{\partial \eta}$$

Letting k*=kb/D, the revised boundary condition at $\eta=1$, $0 \le \xi \le \alpha$ is

$$\frac{\partial W}{\partial \eta} - \frac{mb^2}{aDk*} = 0$$

The second building block has a distributed moment in the supported region expanded as a cosine series. The contribution to moment expanded as a cosine series will thus only have diagonal elements and they will be equal to unity. The only change required to make on the above eigenvalue matrix is to subtract the term 1/k* from the diagonal

slope terms contributed by the second building block. This is shown in figure 6.1. As the stiffness, k*, approaches infinity, we are left with the clamped condition.

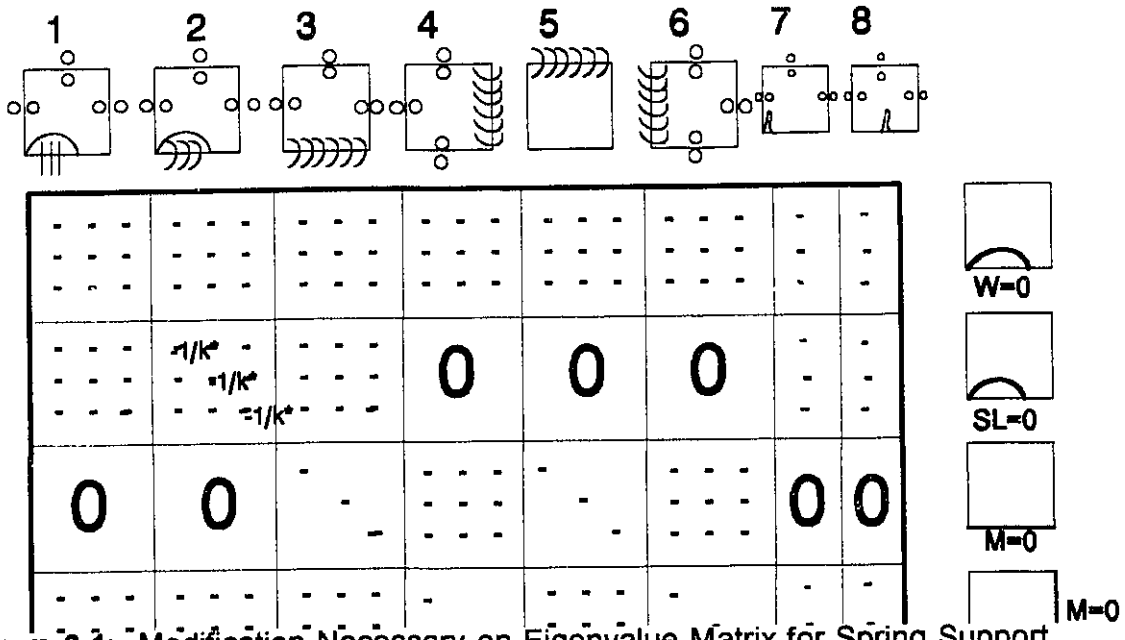

Figure 6.1: Modification Necessary on Eigenvalue Matrix for Spring Support

6.2: Programming Possibilities

The method of superimposing building blocks as demonstrated in this study, often has the advantage of being able to make use of building blocks previously solved for other problems. In this problem only two of the eight building blocks were completely original. The rest were extracted from previously written programs. This reduces the work required for programming, however, the source code must still be inserted and adjusted. It would be useful to have each building block written as separate subroutines so that they could be called into the main program without the risk of introducing bugs. The superposition method generally uses different combinations of familiar building blocks. The choice of appropriate building blocks is the most intuitive step in the

procedure and there may be several possible choices for any given problem. A library of solved building blocks in separately compiled subroutines would make it possible to quickly test different combinations. It may even be possible to write a code that could choose appropriate building blocks for given boundary conditions. The program used to obtain the results presented here, was structured as shown in chapter 4, however, an attempt was made to separate the building blocks. The work was not completed due to time limitations and the lack of direct relevance to this particular study. Only the third building block subroutine was completed successfully. The subroutine must be structured so that it accepts the input parameters and returns the relevant portion of the eigenvalue matrix or the contribution to the displacement. A more suitable programming language may be one which allows dynamic dimensioning so that there would be no need to over dimension the arrays.

6.3: Building Blocks 7 and 8

The necessity of the seventh building block is questionable since the condition of zero slope in the ξ and η directions excludes the possibility of a concentrated force at that extremity of the clamped region. The conditions imposed by this building block do not, however, invalidate the solution. The seventh building block would be useful if the problem is extended to the case of elastically supported edges or plates partially clamped arbitrarily on one edge. The eighth building block is required because there will be a twisting moment induced by the slope in the ξ direction.

6.4: Alternative Building Blocks

As mentioned earlier, there is more then one possible choice of building blocks. To show this, an alternative choice is presented here. It is similar to the above choice but does not have the second building block and the moment in the edge η=1 is only expanded from ξ=α to ξ=1. This choice of building blocks eliminates several Dirac delta functions and may thus converge after fewer terms. The moment in the region from ξ=α to ξ=1 must be expanded to K/2 terms for the eigenvalue matrix to be square.

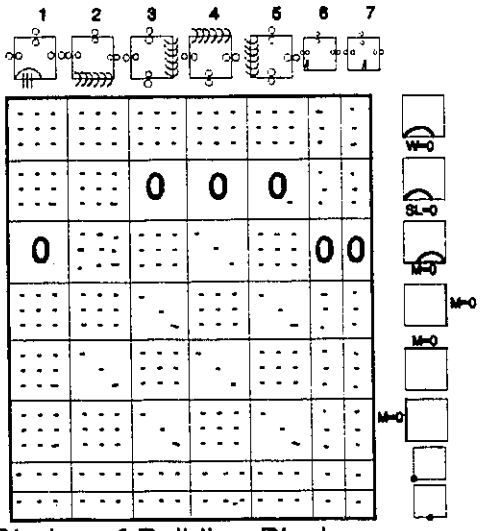

Figure 6.2: Alternative Choice of Building Blocks

The results obtained from this choice of building blocks have to be verified to assess the validity.

6.5: Conclusion

The method presented here for analyzing the free vibration of a partially clamped plate is first analytical solution available to the authors knowledge. The results show good convergence to three digit accuracy. Experimental and finite element method results agree very well with the computed results, confirming the validity. There are practical applications in the area of circuit board vibration. Designers can make use of the eigenvalue and mode shape data to ensure that any probable external harmonic excitationc is out of the resonant frequency range. Mode shape data may be used to avoid placing delicate components at large displacement locations. The method shown is valid for an isotropic thin partially clamped plate of any aspect ratio or clamped length.

References

1. Gorman, D.J. *Free Vibration Analysis of Rectangular Plates*, Elsevier, New York, 1982.

2. Timoshenko, S. and Woinowsky-Krieger S. *Theory of Plates and Shells*, McGraw-Hill, New York 1959.

3. Nowacki, W. *Dynamics of Elastic Systems*, Chapman & Hall Ltd., London, 1963.

4. Leissa, A.W. *Vibration of Plates*, National Aeronatic and Space Association, NASA SP-160, 1969.

5. Ahmed, S. and Banerjee, P.K. "Free Vibration Analysis of BEM using Particular Integrals", *J. Engng Mech.*, ASCE, Vol. 112, pp. 682-695.

6. Brebbia, C.A. *Topics in Boundary Element Research, Volume 2: Time Dependent and Vibration Problems*, Spriger-Verlag, New York, 1985.

7. Szabo, Barno and Babuska, Ivo. *Finite Element Analysis*, John Wiley & Sons, Inc. New York, 1991.

8. Glowinski, R., Rodin, E.Y. and Zienkiewicz, O. *Energy Methods in Finite Element Analysis*, John Wiley & Sons, Inc., Toronto, 1979.

9. Laura, P.A.A. and Grossi, R.O. "Transverse Vibration of a Rectangular Plate Elastically Restrained against Rotation along Three Edges and Free on the Fourth Edge", *Journal of Sound and Vibration*, Vol. 75, pp. 101-107, 1981.

10. Warburton, G.B. and Edney S.L. "Vibrations of Rectangular Plates with Elastically Restrained Edges", *Journal of Sound and Vibration*, Vol. 95, No. 4, pp. 537-552, 1984.

11. Bassily, S.F. and Dickinson S. "On the Use of Beam Functions for Problems of Plates Involving Free Edges", *Journal of Applied Mechanics*, Vol. 42, 858-864, 1975.

12. Tan, C.L. *The Boundary Element Method, A Short Course*, Carleton University, Ottawa, 1987.

13. Gorman, D.J. "An Exact Analytical Approach to the Free Vibration Analysis of Rectangular Plates with Mixed Boundary Conditions", *Journal of Sound and Vibration*, Vol. 93, No. 2, 1984, pp. 235-247.

14. Gorman, D.J. and Singal, R.K. "Analytical and Experimental Study of Vibrating Rectangular Plates on Rigid Point Supports", *AIAA Journal*, Vol. 29, No. 5, 1991, pp. 838-844.

15. Gorman, D.J. "A General Solution for the Free Vibration of Rectangular Plates Resting on Uniform Elastic Edge Supports", *Journal of Sound and Vibration*, Vol. 139, No. 2, 1981, pp.325-335.

16. Gorman, D.J. and Singal, R.K. "Effects of Attached Masses on Free Vibration of Rigid Point Supported Rectangular Plates", *AIAA Journal*, Vol. 30, No. #, 1992, pp. 853-855.

17. Gorman, D.J. "An Analytical Solution for the Free Vibration of Rectangular Plates with Symetrically Distributed Point Supports Along the Edges", *Journal of Sound and Vibration*, Vol. 79, No. 4, 1981, pp. 561-574.

18. Spiegel, Murray R. *Applied Differential Equations*, Third Edition, Prentice-Hall Inc. Englewood Cliffs, New Jersey 1981.

19. Kreyszig, Erwin *Advanced Engineering Mathematics*, Fifth Edition, John Wiley and Sons, New York 1983f.

20. Timoshenko, S. and Goodier, J.N. *Theory of Elasicity*, Third Edition, McGraw-Hill Classic textbook reissue, New York, 1987

21. Orazio, Svelto. *Principles of Laser*, Third Edidition, New York, Plenum Press, 1992.